NASA/TM–2012-208641 / Vol 8

ICESat (GLAS) Science Processing Software Document Series

The Algorithm Theoretical Basis Document for the Atmospheric Delay Correction to GLAS Laser Altimeter Ranges

Thomas A. Herring and Katherine J. Quinn

National Aeronautics and
Space Administration

Goddard Space Flight Center
Greenbelt, Maryland 20771

October 2012

NASA STI Program ... in Profile

Since its founding, NASA has been dedicated to the advancement of aeronautics and space science. The NASA scientific and technical information (STI) program plays a key part in helping NASA maintain this important role.

The NASA STI program operates under the auspices of the Agency Chief Information Officer. It collects, organizes, provides for archiving, and disseminates NASA's STI. The NASA STI program provides access to the NASA Aeronautics and Space Database and its public interface, the NASA Technical Report Server, thus providing one of the largest collections of aeronautical and space science STI in the world. Results are published in both non-NASA channels and by NASA in the NASA STI Report Series, which includes the following report types:

- TECHNICAL PUBLICATION. Reports of completed research or a major significant phase of research that present the results of NASA Programs and include extensive data or theoretical analysis. Includes compilations of significant scientific and technical data and information deemed to be of continuing reference value. NASA counterpart of peer-reviewed formal professional papers but has less stringent limitations on manuscript length and extent of graphic presentations.
- TECHNICAL MEMORANDUM. Scientific and technical findings that are preliminary or of specialized interest, e.g., quick release reports, working papers, and bibliographies that contain minimal annotation. Does not contain extensive analysis.
- CONTRACTOR REPORT. Scientific and technical findings by NASA-sponsored contractors and grantees.
- CONFERENCE PUBLICATION. Collected papers from scientific and technical conferences, symposia, seminars, or other meetings sponsored or co-sponsored by NASA.
- SPECIAL PUBLICATION. Scientific, technical, or historical information from NASA programs, projects, and missions, often concerned with subjects having substantial public interest.
- TECHNICAL TRANSLATION. English-language translations of foreign scientific and technical material pertinent to NASA's mission.

Specialized services also include organizing and publishing research results, distributing specialized research announcements and feeds, providing help desk and personal search support, and enabling data exchange services. For more information about the NASA STI program, see the following:

- Access the NASA STI program home page at http://www.sti.nasa.gov
- E-mail your question via the Internet to help@sti.nasa.gov
- Fax your question to the NASA STI Help Desk at 443-757-5803
- Phone the NASA STI Help Desk at 443-757-5802
- Write to:

  NASA STI Help Desk
  NASA Center for AeroSpace Information
  7115 Standard Drive
  Hanover, MD 21076-1320

NASA/TM–2012-208641 / Vol 8

ICESat (GLAS) Science Processing Software Document Series

The Algorithm Theoretical Basis Document for the Atmospheric Delay Correction to GLAS Laser Altimeter Ranges

Thomas A. Herring
The Massachusetts Institute of Technology, Cambridge, MA
Katherine J. Quinn
The Massachusetts Institute of Technology, Cambridge, MA

National Aeronautics and
Space Administration

Goddard Space Flight Center
Greenbelt, Maryland 20771

October 2012

Level of Review: This material has been technically reviewed by technical management

Available from:
NASA Center for AeroSpace Information
7115 Standard Drive
Hanover, MD 21076-1320

National Technical Information Service
5285 Port Royal Road
Springfield, VA 22161 Price Code: A17

Table of Contents

1.0 Introduction

NASA's Ice, Cloud, and Land Elevation Satellite (ICESat) mission will be launched late 2001. It's primary instrument is the Geoscience Laser Altimeter System (GLAS) instrument. The main purpose of this instrument is to measure elevation changes of the Greenland and Antarctic ice sheets. To accurately measure the ranges it is necessary to correct for the atmospheric delay of the laser pulses. The atmospheric delay depends on the integral of the refractive index along the path that the laser pulse travels through the atmosphere. The refractive index of air at optical wavelengths is a function of density and molecular composition. For ray paths near zenith and closed form equations for the refractivity, the atmospheric delay can be shown to be directly related to surface pressure and total column precipitable water vapor. For ray paths off zenith a mapping function relates the delay to the zenith delay. The closed form equations for refractivity recommended by the International Union of Geodesy and Geophysics (IUGG) are optimized for ground based geodesy techniques and in the next section we will consider whether these equations are suitable for satellite laser altimetry.

To estimate surface pressure and precipitable water vapor, numerical weather models are appealing because they are internally consistent and provide spatially uniform coverage. Values for surface pressure and precipitable water vapor will be calculated from global atmospheric analyses. We will use the National Center for Environmental Prediction (NCEP) global numerical weather analyses. As of January 2000, these analyses are produced on a 1 by 1 degree grid every 6 hours. Fields included are temperature, geopotential height, and relative humidity at standard upper atmospheric pressure levels. These atmospheric fields will be interpolated to the location and time tag of the laser footprints. The NCEP provides a surface pressure field, however error in this field make it unsuitable for our purposes. Surface pressure will be calculated by integrating the upper atmospheric field down to the surface height as given by the initial laser footprint location. Appendix A describes this procedure in detail.

The GLAS single shot error budget assumes less than 20 mm rms error in the atmospheric delay. For all the steps in the atmospheric delay algorithm we require an estimate of the associated error. Unfortunately, NCEP does not provide formal error estimates for its numerical weather models. The atmospheric delay algorithm will be validated using Automatic Weather Station data in polar regions, in-situ meteorological data, where available, at GPS sites, and the estimated delay values from global GPS data. The validation studies performed so far predict less than 12 mm rms error in delay.

Note that all units in this chapter are SI unless otherwise stated.

2.0 Algorithm Description

2.1 Group Refractivity Models

Pulsed satellite laser altimeter systems use the round trip pulse travel time to estimate the distance to the Earth's surface. Atmospheric refraction increases the propagation time and this delay may be corrected for by integrating the refractive index along the ray path through the atmosphere.

The one-way correction to the GLAS range measurement, ΔL, due the refractive effects of the Earth's atmosphere is given by

$$\Delta L = \int_{S_{ATM}} n(s)ds - \int_{S_{VAC}} ds \tag{1}$$

where *n(s)* is the group refractive index of the atmosphere along the ray path, S_{ATM} is the curved path followed by the laser pulse from the space craft to the ground, and S_{VAC} is the straight line path from the space craft to the ground. Evaluation of the second integral only requires the space craft and laser footprint coordinates. Evaluation of the first integral also requires knowledge of the refractive index along the curved ray path and is most accurately calculated using ray tracing or numerical integration methods. This is not practical for large amounts of data, models that relate the total delay to the zenith delay by a mapping function are commonly used such that [*Davis, et al.,* 1985]

$$\Delta L = m(\varepsilon, \boldsymbol{P}) \int_{Z}^{\infty} (n(z) - 1)dz \tag{2}$$

where $m(\varepsilon, \boldsymbol{P})$ is a mapping function that depends on elevation angle, ε, and a parameter vector $\boldsymbol{P}$, and the integral is evaluated along a zenith path from ground point, Z, to the space craft to give the zenith delay. The mapping function will be investigated in a following section.

The argument of the integral, $(n - 1)$ is the refractivity and is normally given in parts-per-million i.e., $(n - 1) = 10^{-6}N$. Refractivity varies in the atmosphere primarily as a function of pressure, temperature, and composition. Precision geodetic surveying requires an accurate knowledge of the group refractive index of air. The first comprehensive set of equations was given by Eldén (1953), these equations were the standard recommended by the International Union of Geodesy and Geophysics (IUGG) for optical wavelengths until recently [*IUGG,* 1963]. Other formulations have been used as new empirical measurements of refractivity have demonstrated errors in the original Eldén equations [*Eldén,* 1966; *Owens,* 1967; *Peck and Reeder,* 1972; *Birch and Downs,* 1994]. A working group of the IUGG has updated their recommendations for the refractive index of air at optical frequencies [*IUGG,* 1999]. There are two solutions recommended, one is a simple closed formula with an accuracy of no better than one part per million and the other is a more complicated algorithm when better that one part per million accuracy is required.

The more accurate algorithm is documented in Ciddor [1996] and Ciddor and Hill [1999]. The Ciddor formulas incorporate the latest moist air refractivity data. They match the measurements within experimental accuracy and are expected to be accurate over a wide range of atmospheric parameters to a few parts in 10^8. The density equations used are valid over ranges of at least -40 to 100 °C, 800 to 1200 hPa, and 0 to 100% relative humidity. However, the algorithm requires a number of steps and as such is unsuitable for practical integration through the atmosphere. It may be used as baseline measurement to compare closed form approximations of refractivity.

The simple closed formula recommended by IUGG is the same as the formula recommended in

1963, amended for an increased CO_2 value of 375 ppm from 300 ppm. This value of carbon dioxide is expected to be valid in 2004 based on estimations of rate of increase and is recommended as the standard value to be used in all formulas. The formula for refractivity is

$$\begin{aligned} N &= N_S \frac{273.15}{1013.25}\left(\frac{P}{T}\right) - 11.27\left(\frac{P_w}{T}\right) \\ N_S &= 287.6155 + \frac{4.88660}{\lambda^2} + \frac{0.06800}{\lambda^4} \end{aligned} \tag{3a}$$

where N is group refractivity, T is temperature (K), P is total pressure (hPa), P_w is water vapor partial pressure (hPa), N_S is standard air refractivity with 375 ppm CO_2, T = 273.15 K, P = 1013.25 hPa, P_w = 0 hPa, λ is wavelength (μm). For the GLAS wavelength of 1.064 μm, and converting pressure units to Pa from hPa, equation 3a becomes

$$N = (0.7871275 \text{ K/Pa})\frac{P}{T} - (0.1127 \text{ K/Pa})\frac{P_w}{T} \tag{3b}$$

The IUGG closed formula is discussed in Rüeger [1996], it was noted that the humidity term is not very accurate and may have other systematic errors. Rüeger strongly recommended that the equations in Owens [1967] be used for higher precision measurements. For optical frequencies, the group refractivity is given by

$$\begin{aligned} N &= k_1(\lambda)\frac{P_d}{T}Z_d^{-1} + k_2(\lambda)\frac{P_w}{T}Z_w^{-1} \\ k_1(\lambda) &= 164.63860\frac{(238.0185 + \lambda^{-2})}{(238.0185 - \lambda^{-2})^2} + 4.77299\frac{(57.362 + \lambda^{-2})}{(57.362 - \lambda^{-2})^2} \\ k_2(\lambda) &= 0.648731 + 0.0174174\lambda^{-2} + 3.55750\times10^{-4}\lambda^{-4} + 6.1957\times10^{-5}\lambda^{-6} \end{aligned} \tag{4a}$$

where $k_1(\lambda)$ and $k_2(\lambda)$ are experimentally determined functions of the laser wavelength (K/Pa), λ is wavelength (μm), P_d and P_w are the partial pressures of dry-air and water vapor (Pa), T is temperature (K), and Z_d and Z_w are the compressibilities of dry-air and water vapor. The Owens equations are based on 300 ppm CO_2. By modifying equation (2) from Ciddor [1996], a correction factor for dry air refractivity based on carbon dioxide concentration may be calculated such that

$$F_C = \frac{N_2}{N_1} = 1 + \frac{(c_2 - c_1)}{(c_1 + 1.8722\times10^6)} \tag{5}$$

where c_1 and c_2 are carbon dioxide concentrations in ppm for the respective dry air refractivity values. For our application, c_1 is 300 ppm and c_2 is 375 ppm, this gives a correction factor of F_C = 1.000040053. Note that this is only applied to the first term in Equation 4a. For the GLAS

wavelength of 1.064 μm, $k_1 = 0.7866070$ K/Pa and $k_2 = 0.6644364$ K/Pa, by also applying the correction for carbon dioxide concentration, equation 4a becomes

$$N = (0.7866385 \text{ K/Pa})\frac{P_d}{T}Z_d^{-1} + (0.6644364 \text{ K/Pa})\frac{P_w}{T}Z_w^{-1} \quad (4b)$$

To approximately compare equation 3b to equation 4b, we will ignore the compressibility factors. Then equation 4b needs re-written in terms of $P_d = P - P_w$. Equation 4b then becomes approximately $N = (0.7866385 \text{ K/Pa})P/T - (0.1222021 \text{ K/Pa})P_w/T$. It can be seen that the two equations are roughly the same. Percentage wise, the constant in front of the water vapor term is the most different, however the water vapor partial pressure is a fraction of the total pressure. The following describes a more quantitative comparison of the two refractivity equations over a range of atmospheric conditions.

The IUGG precision algorithm (Ciddor99) will be used as a baseline to compare the IUGG closed formula (IUGG99) to the modified Owens formula (Owens375). All comparisons will be carried out at a wavelength of 1.064 μm, as appropriate for the GLAS laser altimeter. Setting pressure to 1000 hPa, refractivity is compared over a wide range of temperature and relative humidity and shown in Figure 1. It can be seen that the IUGG99 model performs best for temperatures above 0 ˚C and high humidities. This is not surprising considering that the driving application for the IUGG recommendations is ground based laser geodetic surveying. The modified Owens model performs consistently better for lower temperatures, this suggests that Owens375 is the better model for integration through the atmosphere as the temperature drops through the troposphere.

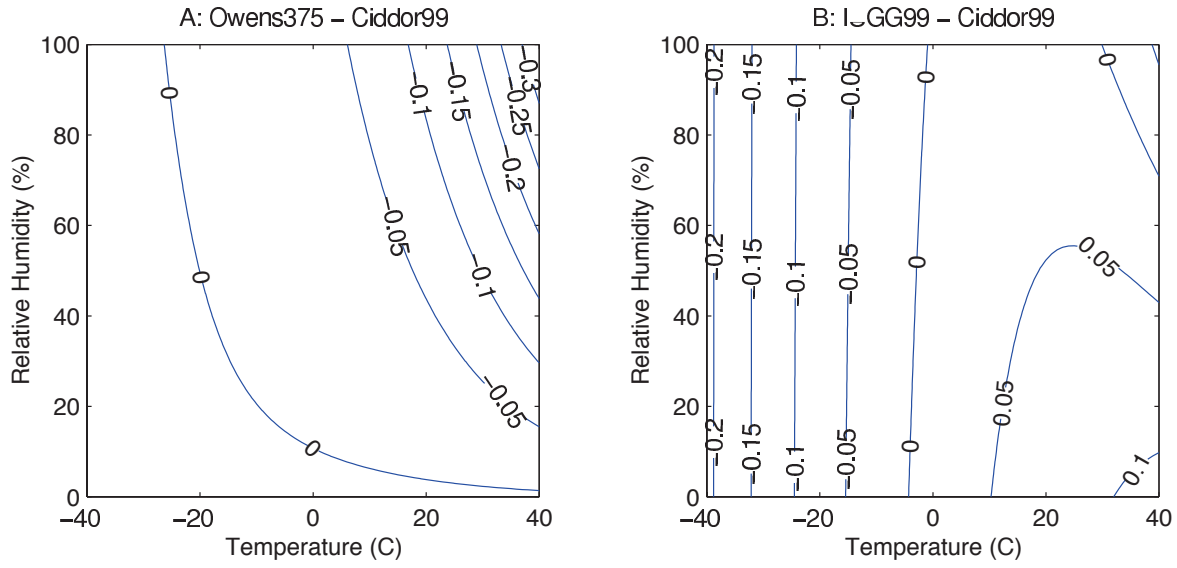

Figure 1. Comparison between closed form models of refractivity and Ciddor99 model, for a constant pressure of 1000 hPa, λ = 1.064 μm.

To assess how the two closed form models perform for satellite laser altimetry we must integrate the differences through the atmosphere. As a point of comparison, we used standard atmospheric profiles for temperature and pressure [*NOAA,* 1976] and varied the relative humidity. The profiles of refractivity were numerically integrated as per Equation 2, setting the mapping function to one to give a zenith delay difference. Figure 2 show profiles for three different values of relative humidity. For zero humidity the modified Owens model is clearly preferable, it becomes less obvious at higher humidities. The integrated difference has been calculated over the whole range of humidities, Figure 3 compares the absolute value of these delay differences. Except for humidities above 80%, the modified Owens model is the preferred model. While the true atmospheric profile will vary from the standard atmosphere and relative humidity is almost certainly not constant along the profile, for satellite altimetry applications the preferred model appears to be Owens375 and will be used for the ICESat mission. Based on the comparison in Figure 3, we can expect inaccuracies in the refractivity model to contribute less than 1 mm to the delay error. It should be noted here that satellite laser ranging (SLR) stations commonly use a refractivity model that is the same form as IUGG99, combined with specialized mapping functions [*Marini and Murray,* 1973], this is the International Earth Rotation Service standard model. We suggest that the standards might be updated to account for the fact that the models currently used are best suited for ground based observations.

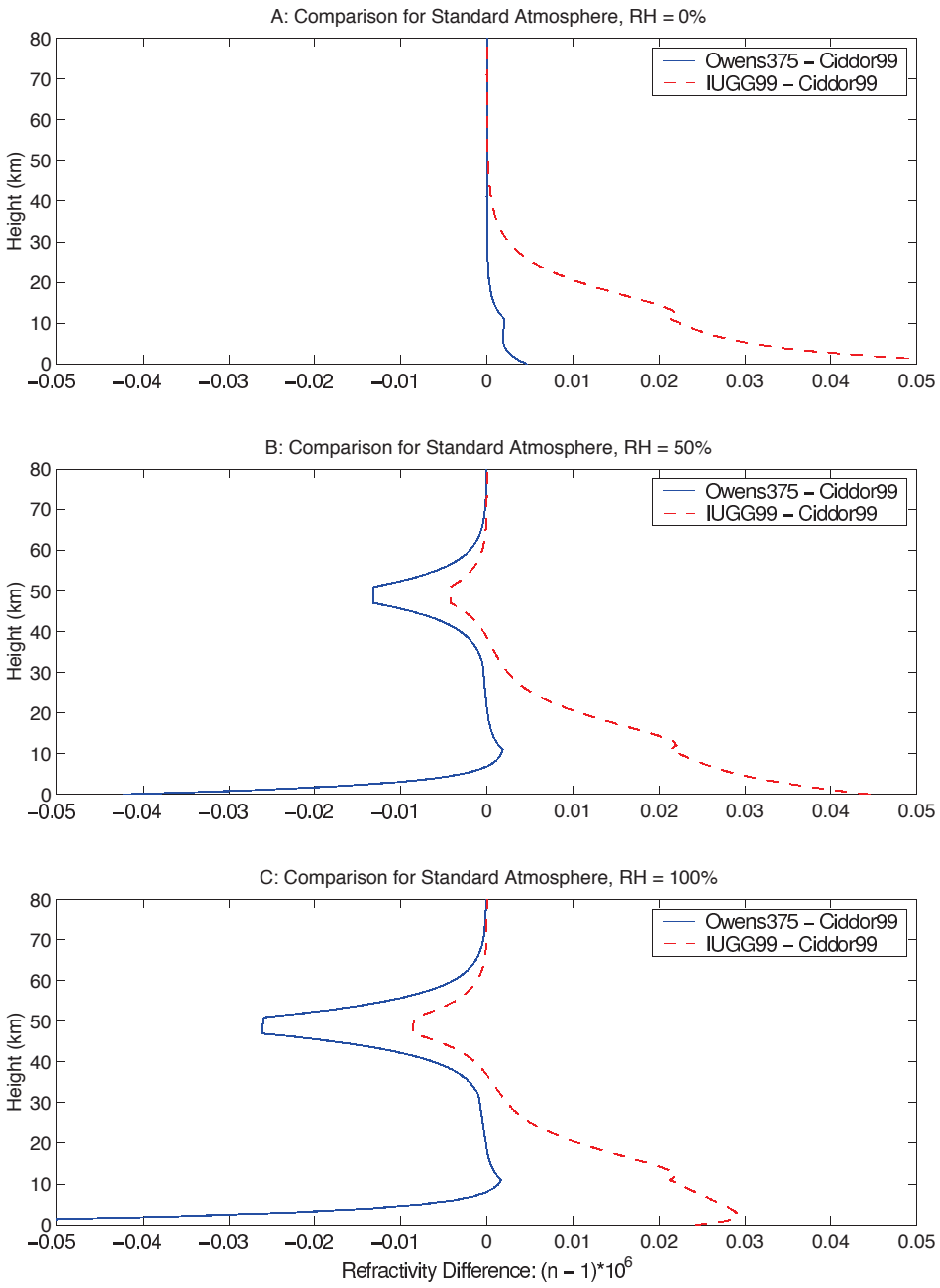

Figure 2. Comparison between closed form models of refractivity and Ciddor99 model, for standard atmosphere profiles of temperature and pressure and varying relative humidity, $\lambda = 1.064\ \mu m$.

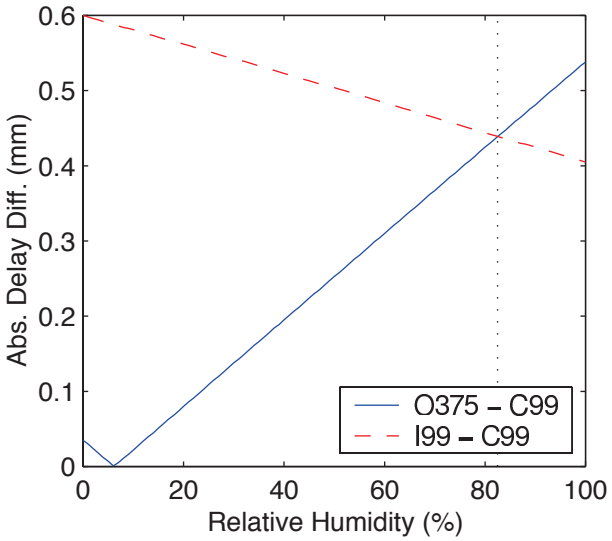

Figure 3. Absolute integrated delay differences between closed form refractivity models and Ciddor99 model, for standard atmosphere profiles of temperature and pressure, $\lambda = 1.064$ μm. Dotted vertical line marks the cross-over point for best model with respect to absolute delay differences.

2.2 Zenith Delay Equations

The modified Owens refractivity equations use compressibilities to account for non-ideal gas behavior such that

$$\rho_i = \frac{P_i}{T}\frac{M_i}{R}Z_i^{-1} \tag{6}$$

where ρ_i is the density of gas i (dry air or water vapor in the case of the atmosphere) with molecular weight M_i and compressibility Z_i, at pressure P_i and temperature T; and R is the Universal gas constant. For reasons that will become clearly shortly, Equation 4 is often combined with Equation 6 and written such that the total density of gas, $\rho = \rho_d + \rho_w$, appears. In this form Equation 4 becomes

$$N = F_c k_1 \frac{R}{M_d}\rho + \left(k_2 - F_c k_1 \frac{M_w}{M_d}\right)\frac{R}{M_w}\rho_w \tag{7}$$

where we have dropped the dependence of k_1 and k_2 on wavelength for simplicity and the dry air refractivity correction factor for carbon dioxide is F_C, as given in Equation 5. The reason for this choice of form for refractivity is that the first term is the largest term and with the assumption that the atmosphere is in hydrostatic equilibrium the integral in Equation 2 for the range correction can be solved exactly. The assumption of hydrostatic equilibrium is violated only under extreme weather conditions, such as thunderstorms and heavy turbulence, where there are significant vertical accelerations [*Fleagle and Businger,* 1980]. These accelerations can reach 1% of gravity,

which correspond to a delay error of approximately 20 mm [*Davis et al.,* 1985], however these extreme conditions are rare and the GLAS laser altimeter will not range through thunderstorms.

We use the hydrostatic equation

$$\frac{dP}{dz} = -\rho(z)g(z) \tag{8}$$

where z is height through the atmospheric column and $g(z)$ is the gravitational acceleration. Substituting Equation 8 into the first term of Equation 7 and then substituting into Equation 2 yields the "hydrostatic" component of the zenith range correction, ΔL_H, which can be written as

$$\Delta L_H = 10^{-6} F_c k_1 \frac{R}{M_d} g_m^{-1} \int_Z^\infty \frac{dP}{dz} dz \tag{9}$$

where g_m is the mean value of gravity in the column of the atmosphere. Since gravity decreases slowly with height and can be closely approximated as a simple function of latitude, this value can be expressed accurately in terms of the height, Z, and latitude, ϕ, of the ground point to which the altimeter measurement is made [*Saastamoinen,* 1972]

$$g_m = 9.8062(1 - 0.00265\cos(2\phi) - 3.1\times10^{-7}(0.9Z + 7300)) \text{ ms}^{-2} \tag{10}$$

Equation 9 can be further reduced because the integral is simply the surface pressure at height Z, and therefore the largest part of the atmospheric range correction in the zenith direction is given by

$$\Delta L_H = 10^{-6} F_c k_1 \frac{R}{M_d} g_m^{-1} P_S \tag{11}$$

where P_s is the surface pressure.

The remaining part of the zenith atmospheric range correction is due to the residual part of the water vapor not included in the hydrostatic term, commonly called the "wet" component, ΔL_W. Substituting the second term of Equation 7 into Equation 2 gives

$$\Delta L_W = 10^{-6} k_2' \frac{R}{M_w} \int_Z^\infty \rho_w dz \tag{12}$$

where $k_2' = k_2 - F_c k_1 \frac{M_w}{M_d}$. The integral is simply the total column precipitable water vapor, *PW*, an atmospheric variable often reported in atmospheric models. The zenith wet delay can now be written as

$$\Delta L_W = 10^{-6} k_2' \frac{R}{M_w} PW \tag{13}$$

When the empirical functions in the refractivity equation given in Owens [1967] are evaluated for the GLAS laser altimeter operational wavelength of 1.064 μm, $k_1 = 0.7866070\,\mathrm{K/Pa}$ and $k_2 = 0.6644364\,\mathrm{K/Pa}$. Dry air with a carbon dioxide concentration of 375 ppm has a molecular weight of M_d = 28.9632 kg.kmol^{-1} [*Ciddor,* 1996], and water has a molecular weight of M_w = 18.0152 kg.kmol^{-1}. Using these values and the previously calculated value for the carbon dioxide correction factor of 1.000040053, $k_2' = 0.1751448\,\mathrm{K/Pa}$. Combining these values and using the Universal gas constant value of R = 8314.510 J.kmol^{-1}.K^{-1} into Equations 11 and 13 gives the final zenith delay equations

$$\Delta L_Z = \Delta L_H + \Delta L_W \tag{14}$$

$$\Delta L_H = (2.2582\,\mathrm{m^2 s^2/Pa}) g_m^{-1} P_S \tag{15}$$

$$\Delta L_W = (8.0834 \times 10^{-5}\,\mathrm{m/mm}) PW \tag{16}$$

Given an average surface pressure value of 1000 hPa and an approximate value of 9.8 ms^{-2} for the mean gravity, the zenith hydrostatic delay is approximately 2.3 m and is the major component of total delay. Zenith wet delay is much more variable, given precipitable water vapor values of less than 10 mm in the polar regions to 50 mm in the tropics, it varies from 1 to 4 mm.

2.3 Off-Nadir Pointing Corrections

The mapping function relates the total atmospheric delay at an arbitrary elevation angle to the zenith delay such that

$$\Delta L = m(\varepsilon, \boldsymbol{P}) \Delta L_Z \tag{17}$$

where ε is the elevation angle and **P** is a vector that commonly consists of various climatological parameters. The mapping function assumes azimuthal symmetry of the atmosphere about the ground point, a very good assumption for the near-nadir pointing ICESat mission, although horizontal gradients are a significant error source for low elevation angle satellite laser ranging.

When it is assumed that the refractivity of the troposphere is azimuthally and spherically symmetric, Marini [1972] showed that the continued fraction form of the mapping function is

$$m(\varepsilon) = \cfrac{1}{\sin\varepsilon + \cfrac{a}{\sin\varepsilon + \cfrac{b}{\sin\varepsilon + \cfrac{c}{\sin\varepsilon + \ldots}}}} \tag{18}$$

where a, b, c, etc., are parameters that may be approximated using climatic data. The very simplest form of this equation is

$$m(\varepsilon) = \frac{1}{\sin\varepsilon} \tag{19}$$

which works best at elevation angles near zenith since that parameters a, b, c, etc., are all significantly less than one. A number of different forms of the mapping function have been published, to test the accuracy of using Equation 19 we will compare this to two different but widely using mapping functions. One is by Davis, et al. [1985], named CfA-2.2, which depends on surface pressure and surface temperature. The other is by Niell [1996] which depends on latitude and day of year. The different climatic variables used are due to the different climatologies and functional forms of the parameters used. We compared the simple mapping function to the test functions by subtracting the test function from the simple mapping function and multiplying by 2.3 m, which is a rough estimate for zenith delay. This gives estimates of how much the total delay will change by. Figures 4 and 5 show these comparisons over a range of climatological conditions.

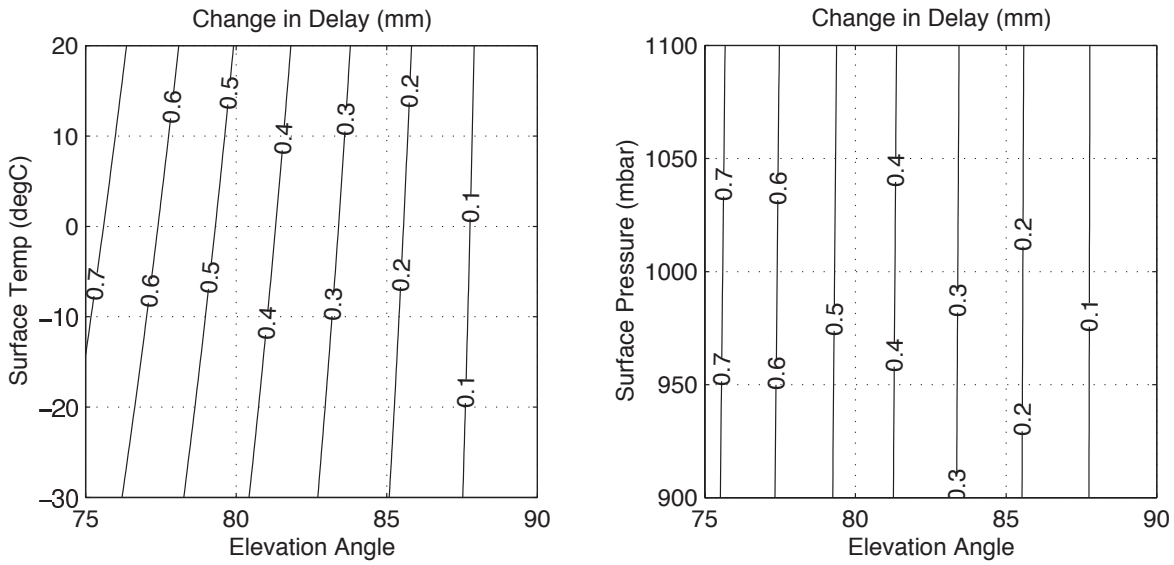

Figure 4. Change in delay of the simple mapping function compared to CfA-2.2 mapping function. Left plot is for P_0 = 1000 mbar, right plot is for T_0 = 0°C.

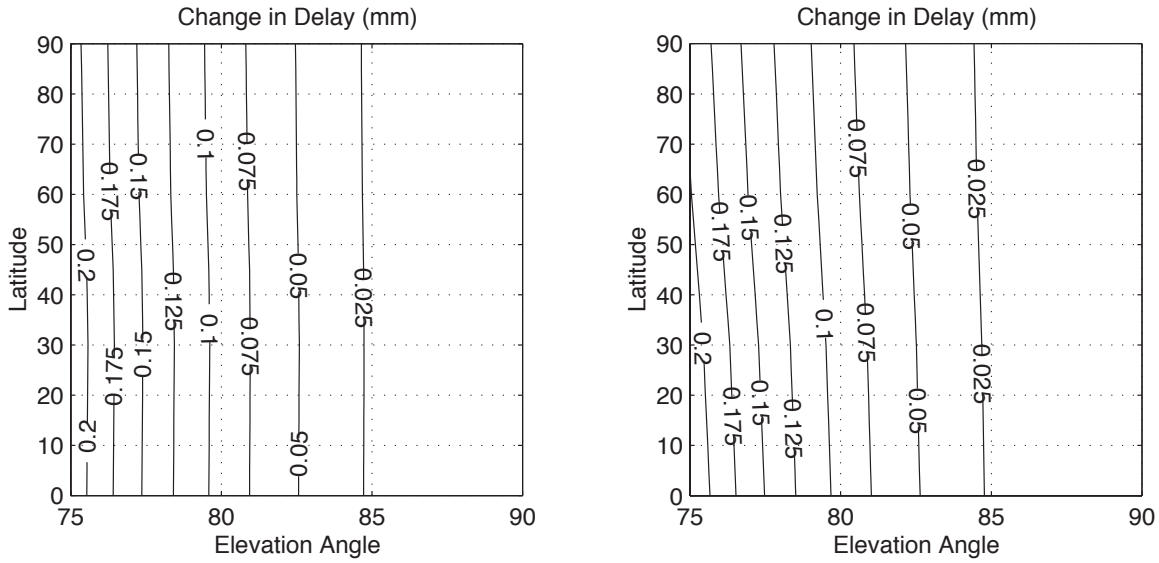

Figure 5. Change in delay of the simple function compared to Niell mapping function. Left plot is for maximum day of year phase, right plot is for minimum day of year phase.

For both of the comparisons, using the simple form of the mapping functions compares very closely to the other forms. We don't expect that the GLAS space craft to point beyond 10° off nadir, the differences in this region are less than 0.5 mm for CfA-2.2 and 0.1 mm for Niell. It should be noted that these other mapping functions are optimized for low elevation angles and in fact we expect the Niell mapping function to work better at higher elevation angles due to its functional form. So we will use the simple $m(\varepsilon) = 1/(\sin\varepsilon)$ form of the mapping function. The error associated with the mapping function should be less than 0.5 mm for pointing angles of less than 10° and decreases to zero for nadir pointing.

There is another concern for off-nadir pointing of the space craft, which is the change in expected footprint location due to bending of the ray in the atmosphere. This effect will not significantly change the atmospheric delay calculation but should be considered for spacecraft pointing calibrations where the location of the laser footprint is directly measured at the ground. The real curved path is shown by the dashed line in Figure 6. P_1 is the expected ground location of the laser footprint for the satellite position and pointing angle, $\alpha_1 = 90^o - \varepsilon_1$, as measured at the satellite. P_2 is the real ground location of the laser footprint after following the refracted path through the atmosphere, which is shifted by a distance d towards the sub-satellite point. If the satellite position and real footprint location were used to calculate the apparent satellite pointing angle, $\alpha_2 = 90^o - \varepsilon_2$, this would be in error by a certain amount such that $\alpha_1 = \alpha_2 - \delta\alpha$. This correction can be approximated by a simple expression for pointing angles of less than 75° [*Astronomical Almanac,* 1999] such that

$$\delta\alpha \;=\; 0.00452° P \tan\alpha_2 / (273 + T) \tag{20}$$

where T is the temperature (°C) and P is the pressure (hPa) at the surface. Using standard surface values of 15°C and 1013 hPa, this gives an approximate value of

$$\begin{aligned} \delta\alpha &= 0.016° \tan\alpha_2 \\ &= 57 \tan\alpha_2 \end{aligned} \tag{21}$$

At an altitude of 600 km and pointing angle of 10 degrees, the pointing error will be approximately 10 arcseconds and the distance the laser footprint is shifted by will be 30 m.

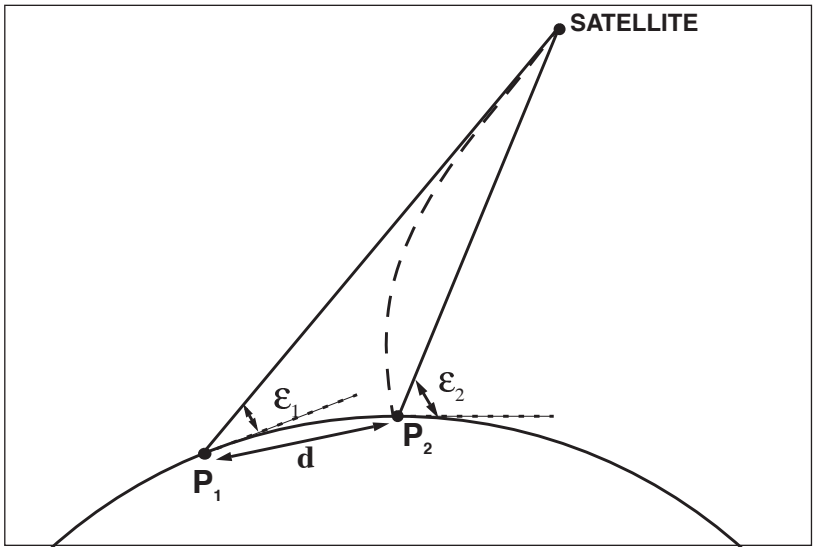

Figure 6. Geometry of laser ray path, dashed line is real path through atmosphere.

As an aside, this correction equation may also be used to estimate whether horizontal gradients in the pressure fields will greatly affect the path of the laser pulse. A typical upper value of the synoptic pressure gradient is 10 mbar per 100 km. Near the surface the derivative of pressure with respect to height is approximately 0.1 hPa/m. This means that a typical slope to the pressure field is 2 arcseconds. Assuming that this gradient is constant through the atmosphere (actually, should decrease exponentially) will can put this angle into Equation 21 to see how much the path will deviate. For a 2 arcsecond slope the deviation is 6×10^{-4} arcseconds, which is entirely negligible.

2.4 NCEP Global Analyses

The zenith delay formulas given in a previous section are directly dependent on surface pressure and total precipitable water vapor. We require a data set that will allow us to calculate values for surface pressure and total precipitable water vapor at the laser footprint locations. Numerical

weather models are appealing because they are internally consistent and provide spatially uniform coverage. We will use the global analyses and forecasts produced by the National Oceanic and Atmospheric Administration (NOAA) National Center for Environmental Prediction (NCEP), the data products are from the Global Data Assimilation System (GDAS) [*Kanamitsu,* 1989; *Kanamitsu et. al.,* 1991].

The NCEP GDAS uses a spectral model based on the primitive atmospheric equations, observational data is assimilated using a spectral statistical-interpolation (SSI) analysis [*Parrish and Derber,* 1992]. Data sources used to create the NCEP global analyses include ground stations, radiosondes, satellites, and buoys. They are produced on 1 degree uniform latitude and longitude grid every 6 hours, starting at 0 GMT. These analyses and forecasts consist of a number of meteorological fields for a standard set of levels from the surface to the stratosphere. The fields that we will use for our surface pressure model are temperature, geopotential height, and relative humidity for the tropospheric pressure levels between 1000 mbar and 300 mbar. The total precipitable water vapor is given as a single field integrated through the entire atmospheric column and may also be calculated by integrating relative humidity through the tropospheric levels.

The NCEP analyses report a surface pressure field, however it is unsuitable for our purposes. The topography field it is produced on has large errors and the spectral interpolation used creates spurious waves in the field near areas of rapid change in elevation, as encountered at the edges of ice sheets. It is essential to perform this integration rather than use the NCEP surface pressure field so that the correct height of the laser footprint is used. We have compared the NCEP surface pressure field with ground station data in Antarctica and found it to be biased by as much as 40 mbar. An atmospheric model of pressure with respect to height is required to reduce the upper level NCEP fields to a surface pressure value. A hydrostatic equilibrium model of the atmosphere is integrated from an upper atmospheric level to the estimated height of the laser footprint in order to calculate surface pressure. This process is described in more detail in the next section. The NCEP global analyses give total column precipitable water vapor as a single field evaluated at the surface, we will use this without modification as input into the zenith wet delay equation. The precipitable water vapor contribution to total delay is small but highly variable both spatially and temporally and should be monitored throughout the ICESAT mission.

The NCEP global analyses can be downloaded near real time from an anonymous NOAA ftp site (ftp.ncep.noaa.gov). It should be noted that this ftp site is not an archive and the products only remain available for approximately 24 hours. Throughout the mission the ICESat team will download and archive the NCEP fields that is required to calculate atmospheric delay.

There are two different runs of the GDAS we will use, based on availability: (a) the final run (FNL); and (b) the aviation run (AVN). The final run produces the best analysis, as it is delayed to allow for late arriving data. The analysis and a 6 hour forecast are posted to the ftp site approximately 6 to 10 hours after the analysis time, the 00Z and 12Z analyses take longer than the 06Z and 18Z analyses because there are more ground station data taken on 12 hour intervals. The aviation run uses exactly the same model as the final analysis except that it is run at an earlier time and therefore has less data included, the AVN analysis is posted to the ftp site approximately 3.5 hours after the analysis time. The forecasts are every 6 hours out to 84 hours and take an additional 5 minutes to be posted for each forecast, all forecasts are posted to the ftp site approxi-

mately 5.5 hours after the analysis time. Table 1 is a summary of approximate NCEP delivery times.

Over 95% of the time, the final analysis is available for use. However, sometimes this run is not performed by NCEP due to time constraints. Our next best choice is the aviation analysis, which is almost always available. If the analyses are not available we will use the forecasts, the order of preference being the FNL 6 hour forecast, then the AVN forecasts in ascending time. The atmospheric delay estimates should be flagged according to the data used, in order to assess the quality of the estimate. The forecasts need to be archived until it is certain we can obtain the better analyses.

Table 1: NCEP Delivery Times as of March 29, 2000

Model	0000Z	0600Z	1200Z	1800Z
FNL				
analysis	0730Z	1030Z	2130Z	2300Z
6 hr forecast	0735Z	1035Z	2135Z	2305Z
AVN				
analysis	0315Z	0920Z	1515Z	2115Z
6 hr forecast	0325Z	0930Z	1525Z	2125Z
84 hr forecast	0405Z	1010Z	1605Z	2205Z

The NCEP products are stored in GRIB format (GRIdded Binary). This format is widely used in the meteorological community and is the World Meteorological Organization standard for exchanging gridded binary data. It is thoroughly described by NCEP Office Note 388 [*Stackpole,* 1994]. NCEP has codes for reading GRIB format that we have incorporated into our atmospheric delay software package.

Unfortunately, there are no formal error estimates provided for the atmospheric fields produced by the NCEP GDAS. Studies have compared analyses produced by different forecasting centers, notably the European Center for Medium-Range Weather Forecasting (ECMWF), however these competing analyses use much the same input data and physical models and as such do not provide a quantitative error estimate [*Trenbreth & Olsen*, 1988; *Boer et al.,* 1992]. Validation studies have been performed for the surface pressure and precipitable water vapor estimates to address this shortfall.

2.5 Surface Pressure

An atmospheric model of pressure with respect to height is required to reduce the upper level NCEP fields to a surface pressure. To simplify the physical model of the atmosphere we will make certain assumptions. A static atmosphere model will allow us to consider the vertical distribution of atmospheric variables. Although the atmosphere is actually a dynamic system, static atmosphere formulas for variables like pressure and density are valid to a high degree of accuracy. We will assume a horizontally stratified atmosphere in hydrostatic equilibrium, such that pressure is related to height by the hydrostatic equation

$$dP = -g(Z)\rho(Z)dZ \tag{22}$$

where Z is geometric height, P is pressure, g is gravity, and ρ is density.

To allow easier integration of this equation, we will convert geometric height into geopotential height. A geopotential meter is defined as the work done by lifting a unit mass one geometric meter through a region in which gravity is uniformly 9.80665 m/s^2, the value of mean sea level gravity. The geopotential measured with respect to mean sea level (assumed zero potential) is called geopotential height, H, such that

$$H = \frac{1}{g_0}\int_0^Z g\,dz \tag{23}$$

where g_0 = 9.80665 m^2/s^{2}m' [NOAA, 1976]. The derivative of this equation with respect to geometric height is

$$g_0 dH = g\,dZ \tag{24}$$

This can be substituted into the hydrostatic equation to give

$$dP = -g_0\rho(H)dH \tag{25}$$

We now require an expression that will convert elevation in geometric meters to geopotential meters. This will be related to the variation of gravity with height. Approximating the Earth as a sphere with only radial mass variations, gravity is inversely proportional to radius squared, which will give a conversion equation of

$$g = g_{msl}\left(\frac{R^2}{(R+Z)^2}\right) \tag{26}$$

where R = 6371009 m is mean radius of the Earth, g_{msl} is gravity at mean sea level. Substituting this equation for gravity into Equation (23) gives the conversion formula

$$H = \frac{g_{msl}}{g_0}\frac{RZ}{(R+Z)} \tag{27}$$

Mean sea level gravity depends on geodetic latitude, the formula is based on calculations of the standard geodetic refence system [Moritz, 1980] such that

$$g_{msl} = g_{eq}(1 + k\sin^2\phi)(1 - e^2\sin^2\phi)^{-\frac{1}{2}} \tag{28}$$

where ϕ is latitude, $g_{eq} = 9.7803267715$ m/s^2, $k = 0.001931851353$, $e^2 = 0.00669438002290$.

Many atmospheric models, such as the U.S. Standard Atmosphere [NOAA, 1976], simplify their calculations for pressure by assuming the air to be a dry, ideal gas. We shall include non-ideal gas effects and water vapor partial pressure. The equation of state for a pure non-ideal gas is

$$Z^{-1}\frac{PV}{RT} = \frac{m}{M} \tag{29}$$

where Z^{-1} is called the inverse compressibility and depends empirically on pressure and temperature [Harrison, 1965b], P is pressure, V is volume, R is the universal gas constant, T is temperature, m is mass, and M is molecular weight.

Density can be written as $\rho = m / V$, and we can split mass components of water and dry air: $m = m_w + m_d$. If we assume that moist air obeys Dalton's Law of partial pressures, the separate masses can be evaluated by the non-ideal equation of state to give a density equation of

$$\rho = \frac{1}{RT}(Z_w^{-1} P_w M_w + Z_d^{-1}(P - P_w) M_d) \tag{30}$$

where $R = 8314.510$ J/kmol.K, $M_w = 18.0152$ kg/kmol, $M_d = 28.9632$ kg/kmol for 375 ppm carbon dioxide concentration, P is the total pressure and P_w is the partial pressure of the water vapor in the air. It is implicitly assumed that the dry air components are homogeneously mixed throughout the lower atmosphere and therefore the mean molecular weight of dry air is a constant.

Equations for inverse compressibility have been experimentally determined by Owens [1967], these formulas are accurate to within a few parts per million

$$Z_w^{-1} = 1 + 1650\frac{P_w}{T^3}[1 - 0.01317(T - 273.15) + 1.75\times10^{-4}(T - 273.15)^2 + 1.44\times10^{-6}(T - 273.15)^3] \tag{31}$$

$$Z_d^{-1} = 1 + (P - P_w)\left[57.90\times10^{-8}\left(1 + \frac{0.52}{T}\right) - 9.4611\times10^{-4}\frac{(T - 273.15)}{T^2}\right] \tag{32}$$

We need an equation for water vapor pressure. Given sufficient saturation vapor pressure data over a wide range of temperature, the information can be stored in an analytical form. One of the better forms uses Chebyshev polynomials [McGarry, 1983]

$$T \log_{10}\left(\frac{P_s}{P_b}\right) = \frac{a_o}{2} + \sum_{s=1}^{n} a_s E_s(x) \tag{33}$$

where P_b = 1000 Pa, P_s is saturation vapor pressure, $E_s(x)$ are Chebyshev polynomials:

$$\left.\begin{aligned} E_0(x) &= 1 \\ E_1(x) &= x \\ E_{s+1}(x) &= 2xE_s(x) - E_{s-1}(x) \\ x &= \frac{2T - (T_{max} + T_{min})}{T_{max} - T_{min}} \end{aligned}\right\} \tag{34}$$

The coefficients a_s (s = 0,...,10) are a_s = {2794.027, 1430.604, -18.234, 7.674, -0.022, 0.263, 0.146, 0.055, 0.033, 0.015, 0.013}, T_{max} = 648 K, and T_{min} = 273 K [Ambrose, 1987].

To get the water vapor pressure from the saturation vapor pressure we use relative humidity [Harrison, 1965a]

$$P_w = RhP_s \tag{35}$$

where relative humidity is in a fractional form with values between 0 and 1. Actually, this equation is only true for pure water vapor, *not* moist air. However the equation is approximately true for moist air. Note that the World Meteorological Organization (WMO) has adopted the practice of evaluating relative humidity with respect to liquid water at all temperatures, even those below 0 °C.

We now have an expression for density that depends on temperature, relative humidity and pressure. To solve the hydrostatic equation we must express temperature and relative humidity as functions of geopotential height, in order to get an expression for density that only depends on geopotential height. The NCEP global analyses have values for temperature, geopotential height and relative humidity at standard pressure levels. We shall assume that temperature varies linearly with respect to geopotential height between these levels, a relatively good assumption for the lower atmosphere such that

$$T = T_0 + L(H - H_0) \tag{36}$$

$$L = \frac{T_1 - T_0}{H_1 - H_0} \tag{37}$$

where L is the temperature gradient; T_0 and H_0 are temperature and geopotential height at the upper level; T_1 and H_1 are temperature and geopotential height at the lower level: $H_1 < H \leq H_0$.

We will also assume that relative humidity varies linearly with respect to geopotential height between levels such that

$$Rh = Rh_0 + S(H - H_0) \tag{38}$$

$$S = \frac{Rh_1 - Rh_0}{H_1 - H_0} \tag{39}$$

where S is the relative humidity gradient, Rh_0 is relative humidity at the upper level, Rh_1 is relative humidity at the lower level. Given these expressions for temperature and relative humidity, the hydrostatic equation becomes

$$\frac{dP}{dH} = -\frac{g_0}{RT}[Z_v^{-1}(H)P_v(H)M_v + Z_a^{-1}(H, P)[P - P_v(H)]M_a] \tag{40}$$

This differential equation is first order, non-linear and inhomogeneous, we are not able find an analytic solution. To obtain a numerical solution for pressure we will numerically integrate down from the upper level geopotential height to the desired geopotential height. Pressure varies smoothly with geopotential height, this means that we are relatively unrestricted in our choice of numerical method. We will use the Bulirsch-Stoer method, this method is one of the best ways to obtain high accuracy solutions with minimal computational effort, so long as integrated function is smooth and has no singular points within the range of integration (Press *et al*., 1989).

2.6 Precipitable Water Vapor

The NCEP global analyses give total column precipitable water vapor as a single field evaluated at the surface, we will use this without modification as input into the zenith wet delay equation. The precipitable water vapor contribution to total delay is small but highly variable both spatially and temporally and should be monitored throughout the ICESAT mission.

To validate the precipitable water vapor fields we will compare them to ground station data. One of resources we will use is the GPS global network. Precipitable water vapor can be derived from estimates of GPS tropospheric delay made at each global station. This derivation requires the knowledge of surface pressure at the station. There are over 35 GPS stations that report surface pressure from on site met packages, however only two of these are in the polar regions, both in the north. Where directly measured surface pressure is unavailable we can use our own surface pressure model without a significant loss of accuracy. There are currently 4 stations in Antarctica and 6 stations in the Arctic where we can make precipitable water vapor measurements. The major advantage of using the GPS global network is the rapid availability of data and confidence that the data will be available over the length of the ICESAT mission.

2.7 Delay Correction with Respect to Height

As can be seen in the previous sections, calculation of the surface pressure and therefore delay requires a knowledge of the height of the laser footprint location. The atmospheric delay correction will be estimated early in the GLAS processing and there may be later adjustments to the

spacecraft orbit and footprint location height. We need a simple correction function that would be accurate for height changes in the range of ±100 m.

Given that pressure varies approximately exponentially with height, we expect the correction to be of the form

$$P' = Pe^{(-A(H' - H))} \tag{41}$$

where *P'* and *H'* are the corrected pressure and geopotential height, *P* and *H* are the original pressure and geopotential height, and *A* is the correction parameter.

Neglecting water vapor, the hydrostatic equation becomes

$$\frac{dP}{dH} = \frac{-g_0 Z_d^{-1} P M_d}{RT} \tag{42}$$

Assuming that temperature and inverse compressibility are a constant with respect to height lets us solve Equation 42 for the correction factor such that

$$A = \frac{g_0 Z_d^{-1} M_d}{RT} \tag{43}$$

where *P, T,* and Z_d^{-1} are calculated at the original height. For typical surface values for temperature of 273.15 K, given g_0 = 9.80665 m^2/s^2.m' [NOAA, 1976], and neglecting the compressibility factor, A = 1.25 x 10^{-4} m^{-1}. This correction factor is defined for geopotential meters, it may be converted to geometric meters using mean sea level gravity instead of g_0. Since atmospheric delay is directly proportional to surface pressure, again neglecting water vapor, this same correction factor may be applied such that

$$\Delta L' = \Delta L e^{(-A(H' - H))} \tag{44}$$

2.8 Spatial Interpolation

The NCEP global analyses we will use are given on a 1 by 1 degree uniform latitude and longitude grid. We require an interpolation scheme that will allow us calculate the atmospheric field values at the laser footprint locations. This interpolation method will have to be computationally efficient to keep up with the real time data processing requirements. The global analyses have the highest realistic spatial resolution by design, therefore a complicated interpolation scheme intended for sparse data sets would not be useful nor appropriate. The upper level fields of temperature, geopotential height and relative humidity are quite smooth, a bilinear interpolation of the grid will be sufficient. The precipitable water vapor field is much more variable, however its accuracy and small contribution to the total delay do not warrant anything more complicated than bilinear interpolation as well.

Bilinear interpolation has the form

$$\begin{aligned} f(\phi, \lambda) &= a + bX + cY + dXY \\ a &= f(\phi_1, \lambda_1) \\ b &= f(\phi_1, \lambda_2) - f(\phi_1, \lambda_1) \\ c &= f(\phi_2, \lambda_1) - f(\phi_1, \lambda_1) \\ d &= f(\phi_1, \lambda_1) + f(\phi_2, \lambda_2) - f(\phi_1, \lambda_2) - f(\phi_2, \lambda_1) \\ X &= (\lambda - \lambda_1) / (\lambda_2 - \lambda_1) \\ Y &= (\phi - \phi_1) / (\phi_2 - \phi_1) \end{aligned} \tag{45}$$

where f is the field value, ϕ is latitude, λ is longitude. The subscripts 1 and 2 stand for south and north latitudes and the west and east longitudes of the four known grid points directly surrounding the unknown point.

Any errors that arise from using bilinear interpolation will be included in the errors estimated in our validation studies. To estimate errors that arise purely from the bilinear interpolation, we decimated the 1 by 1 degree NCEP grid to 2 by 2 degrees, then interpolate back to the original grid. The interpolated values were then differenced from the original 1 by 1 degree grid values. This will give an upper bound on the interpolation errors, as we are using a coarser grid to interpolate. The field we will use for testing is the 1000 hPa geopotential height field (GPH). This is the most appropriate field to use, considering the surface pressure algorithm integrates from an interpolated upper atmospheric GPH fields down to the surface. Average global surface pressure is approximately 1013 hPa, therefore the 1000 hPa GPH field is the one most likely to be used in the surface pressure algorithm. The error in the GPH field can then be approximately converted to delay error using the 0.29 mm of delay to 1 meter height change correspondence. Tests indicate that the spatial interpolation error for the 1000 hPa GPH field, zonally averaged, is no more than 7m, corresponding to 2 mm of atmospheric delay.

2.9 Temporal Interpolation

The NCEP fields used to model atmospheric delay are only produced every 6 hours. To estimate delay values at the times of the laser pulses we will need to temporally interpolate between the NCEP output times. Surface pressure is the major contributor to atmospheric delay, we can look at the temporal behavior of surface pressure to guide our temporal interpolation scheme. Spectral plots of surface pressure are used to characterize the statistical properties of the time series. For example, if a log-log plot of power spectral density versus frequency is has a slope of -2 then the time series can be described as a random walk process. For these processes, the maximum likelihood interpolator is simply a linear interpolation between adjacent points.

Surface pressure time series from automatic weather stations (AWS) in Antarctica were used to calculate power spectral density plots. Stations were chosen that had 2 years of largely uninterrupted time series. The AWS data used had a sampling period of 10 minutes, short gaps in the data were bridged was linear interpolation. Analysis of the power spectra show that log-log plots

of these spectra fall off at high frequencies with an approximate slope of -2.5, if some of the white noise tail is ignored. This slope is close to -2, therefore consistent with a random walk stochastic process.

The power spectral density plots for the higher temporal resolution AWS data may be used to estimate how much variance in surface pressure we are missing by using the coarser resolution NCEP fields. The additional variance is the power integrated under the power spectral density plots for frequencies higher than the NCEP nyquist frequency. The current NCEP global analyses are produced every 6 hours, therefore the nyquist frequency is 2 cyc/day. The additional integrated power was no more than 0.1 hPa for the AWS stations examined. This corresponds a delay error of no more than 0.3 mm due to the temporal resolution of the NCEP fields, which is negliable compared to the 20 mm error budget and other error sources.

2.10 Coordinate Systems

The calculation of atmospheric delay at the laser footprint locations requires knowledge of the footprint latitude, longitude, and initial height estimate. The laser footprint coordinates are given as geodetic latitude, longitude, and height above ellipsoid [*Schutz,* 1999]. The reference ellipsoid used is WGS-84, defined by semi-major axis (a = 6378137.0 m), semi-minor axis (b = 6356752.3142 m), first eccentricity squared (e^2 = 0.00669437999013) [*NIMA,* 1997]. However all of the atmospheric data from NCEP are referenced to orthometric height, i.e. height above geoid. We need to convert the laser footprint ellipsoid height to height above geoid. The height difference can range from -100 m to 100 m, leading to a delay difference of approximately 23 mm to -23 mm. To calculate orthometric height we need to know the value of the geoid at the footprint location. Let H be the orthometric height, h be the ellipsoid height, and N_g be the geoid value. Then the height conversion is

$$H = h - N_g \tag{46}$$

The geoid values are calculated using the National Imagery and Mapping Agency 30 arc-minute geoid grid as defined for WGS-84 [*NIMA*, 1997], which is interpolated using bilinear interpolation to the footprint locations.

2.11 Processing Flow

There are two separate processes for calculating the atmospheric delays. The “background” process is the archiving of the required NCEP data. This data should be archived on-site as it is only posted to the NOAA ftp site for 24 hours before being replaced by the next day’s data. Once the required fields are extracted, the daily volume of data, as of March 2000, is 25.8 Mbytes. The main process is the calculation of the delays. The timing of the delay calculation is driven by two data streams: the NCEP fields and the laser ranges. We wish to calculate the delays within 12 hours of real time, if the laser ranges are available in a timely fashion then the biggest impediment to delay processing is the up to 9.5 hour time lag on the 12Z FNL analysis field (Table 1). The following processing flow assumes that the laser range data is available on a much shorter time lag than the NCEP fields. All the processing is done in 6 hour time blocks, as this is the time step of the NCEP fields.

Let t_1 be a given 6 hourly time step, let t_2 be the next time step. Let P_{12} be a set of all laser ranges with a time tag, t, such that $t_1 \leq t < t_2$.

1. Between t_1 + 5 hr and t_1 + 9.5 hr: Access NCEP fields for t_1. If FNL analysis is archived on-site, proceed. If not archived, attempt to retrieve from the NOAA ftp site. If not available, use the next best analysis for forecast.

2. Next: Calculate delays for P_{01} at time value t_1.

3. Next: Interpolate with respect to time delays for P_{01} at t_0 and P_{01} at t_1. (Note, delays for P_{01} at t_0 were calculated in the previous loop of this process). Save these delay values.

4. Next: Calculate delays for P_{12} at time value t_1. Do these calculations as soon as laser ranges come in, make sure completed before next time step.

5. Repeat for next time step (t_2).

3.0 Validation

The error budget set out in the GLAS science requirements assumes less than 20 mm single shot total atmospheric delay error. Total zenith delay basically consists of two components, zenith hydrostatic delay (ZHD) and zenith non-hydrostatic or "wet" delay (ZWD). Examples of total zenith atmospheric delay in the polar regions, as calculated by our model on the NCEP grid, are given in Figures 7 and 8. ZHD is the major component, there is approximately 2.3 mm of delay per millibar with a typical value of 2.3 m. Wet delay is much smaller but more variable, there is approximately 0.08 mm of delay per kg/m^2 of precipitable water vapor. Typical values in the polar regions are less than 1mm of delay and up to 6 mm of delay in the tropics.

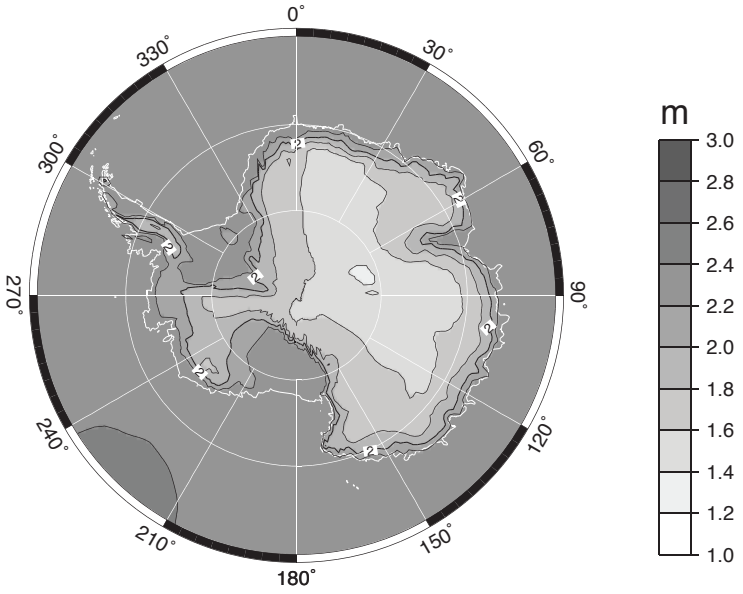

Figure 7. Atmospheric delay for Antarctica, 0 GMT January 1, 1998.

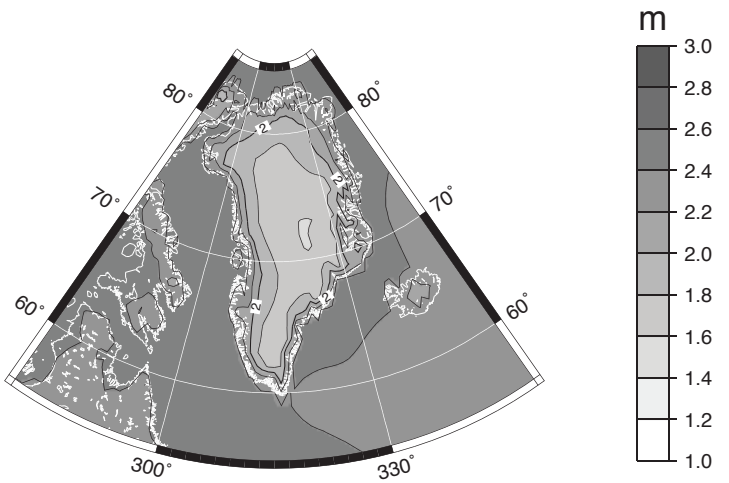

Figure 8. Atmospheric delay for Greenland, 00 GMT January 1, 1998.

To validate the atmospheric delay estimate requires that we validate our surface pressure and precipitable water vapor estimates, especially in the polar regions. Sources of readily obtainable surface pressure measurements are Automatic Weather Stations (AWS) in Antarctica and Greenland [*Sterns and Wendler*, 1988; *Steffen et al*, 1996], and GPS stations with meteorological packages. Comparisons of model estimates with polar AWS's for 2 year's worth of data in 1998 and 1999 show an rms error of less than 5 hPa once a mean offset is removed, the majority have less than 3 hPa rms error. The offset removal is justified as the station heights are not accurately known. These rms surface pressure errors correspond to delay errors of less than 12 mm, usually less than 7 mm, which is less than the 20 mm error budget. Two examples of these comparisons are given in Figure 9. Errors estimates are also a combination of model errors and ground station errors, the AWS barometers are theoretically calibrated to +/- 0.2 hPa.

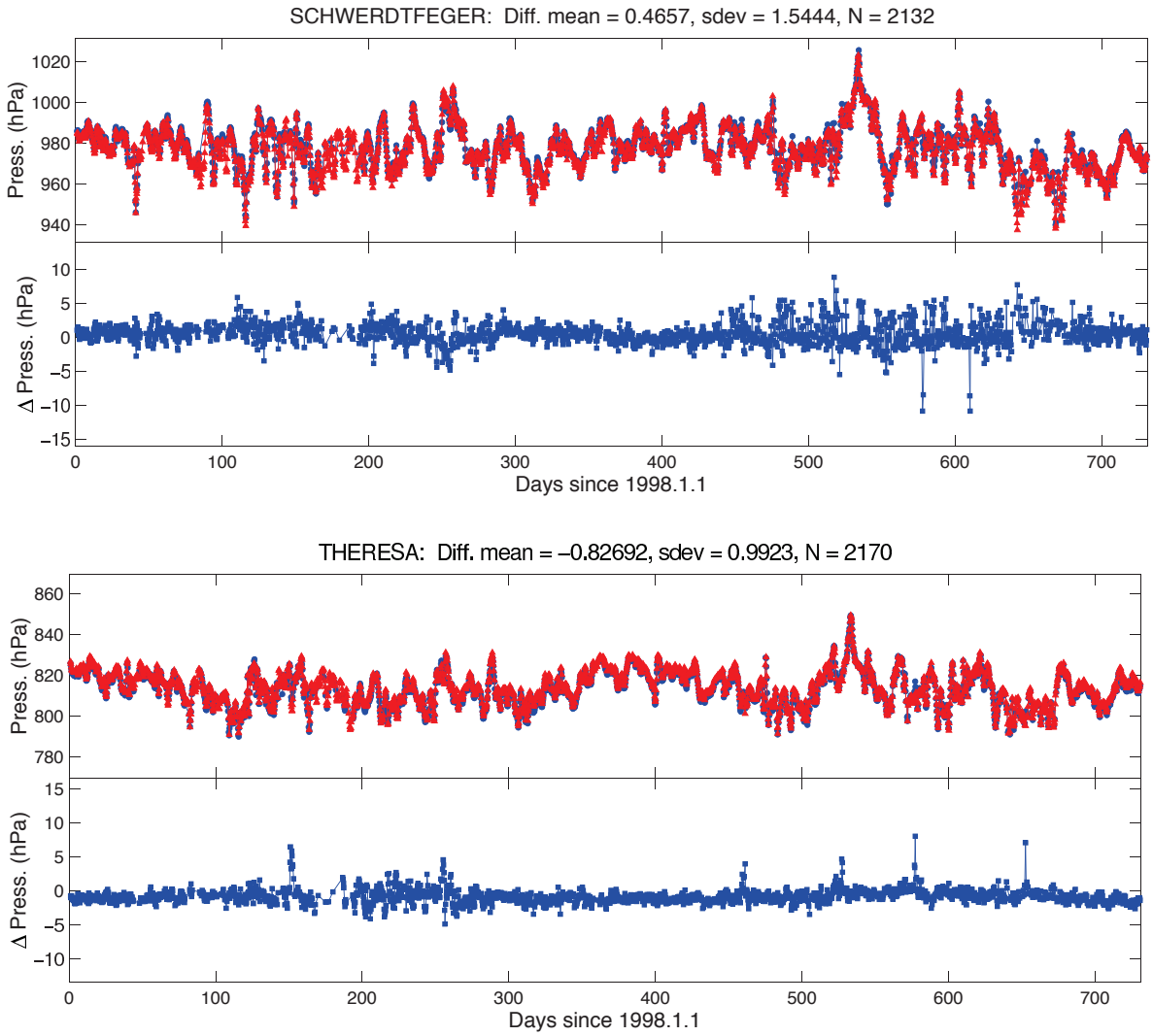

Figure 9. Schwerdtfeger AWS, Ross Ice Shelf, and Theresa AWS, West Antarctica. Upper plot for each station shows NCEP surface pressure values (squares) and AWS values (triangles). Lower plot is surface pressure differences, NCEP minus AWS.

Precipitable water vapor data are harder to come by, however the technique of GPS meteorology can provide some data [*Quinn and Herring*, 1999]. GPS processing produces an estimate of total delay at microwave wavelengths, which is much more sensitive to water vapor than optical wavelengths. If the surface pressure at the GPS station is known then precipitable water vapor estimates can be derived. If the station does not have an on-site met package then our NCEP surface pressure model may be used, greatly increasing the amount of available data. The error from using NCEP surface pressure is approximately 2 mm of precipitable water vapor (PW). We have used this method for 4 GPS stations in Antarctica and 2 in Greenland that are part of the IGS global network. Figure 10 shows the results of this technique, comparisons of GPS derived estimates

of PW versus NCEP global atmospheric model estimates of PW for a 2 week period in November 1998. From top to bottom in the figure, the four Antarctic stations are Casey (CAS1), Davis (DAV1), McMurdo (MCM4), and O'Higgins (OHIG), the two Greenland stations are Kangerlussuaq (KELY), and Thule (THU1).

First of all, it can be seen that for all the stations, except for McMurdo, the NCEP PW value is on average less than the GPS PW value. This may be because radiosonde humidity sensors tend to underestimate the true value in cases of very cold temperature and low humidities, both being true in the polar regions. Within the 2mm error bars for the GPS values, some NCEP values track reasonably well, i.e. Casey and Thule. The worst fitting station is O'Higgins where the NCEP values are too low and too smooth. In fact for all the stations the NCEP values appear to be too smooth. The rms errors are all less than 4 mm of precipitable water vapor, which corresponds to 0.3 mm of delay, which is almost negliable and of the same order as the measurements themselves. However, one concern is that there may be seasonal variations in the bias and error that would show up as seasonal variations in ice thickness. Another is that changes in the NCEP Global Data Assimilation System may show steps in the values as resolutions and data sources change. Therefore we will continue to model the wet delay and moniter its errors.

The surface pressure and precipitable water vapor validation will be continuously performed and monitered over the lifetime of the GLAS mission. In summary, results so far indicate that the surface pressure error in polar regions is less than 5 mbar or 12 mm delay. Precipitable water vapor errors in polar regions are less than 5 kg/m2 or 0.4 mm delay. These errors are less than the 20 mm error budget assumed.

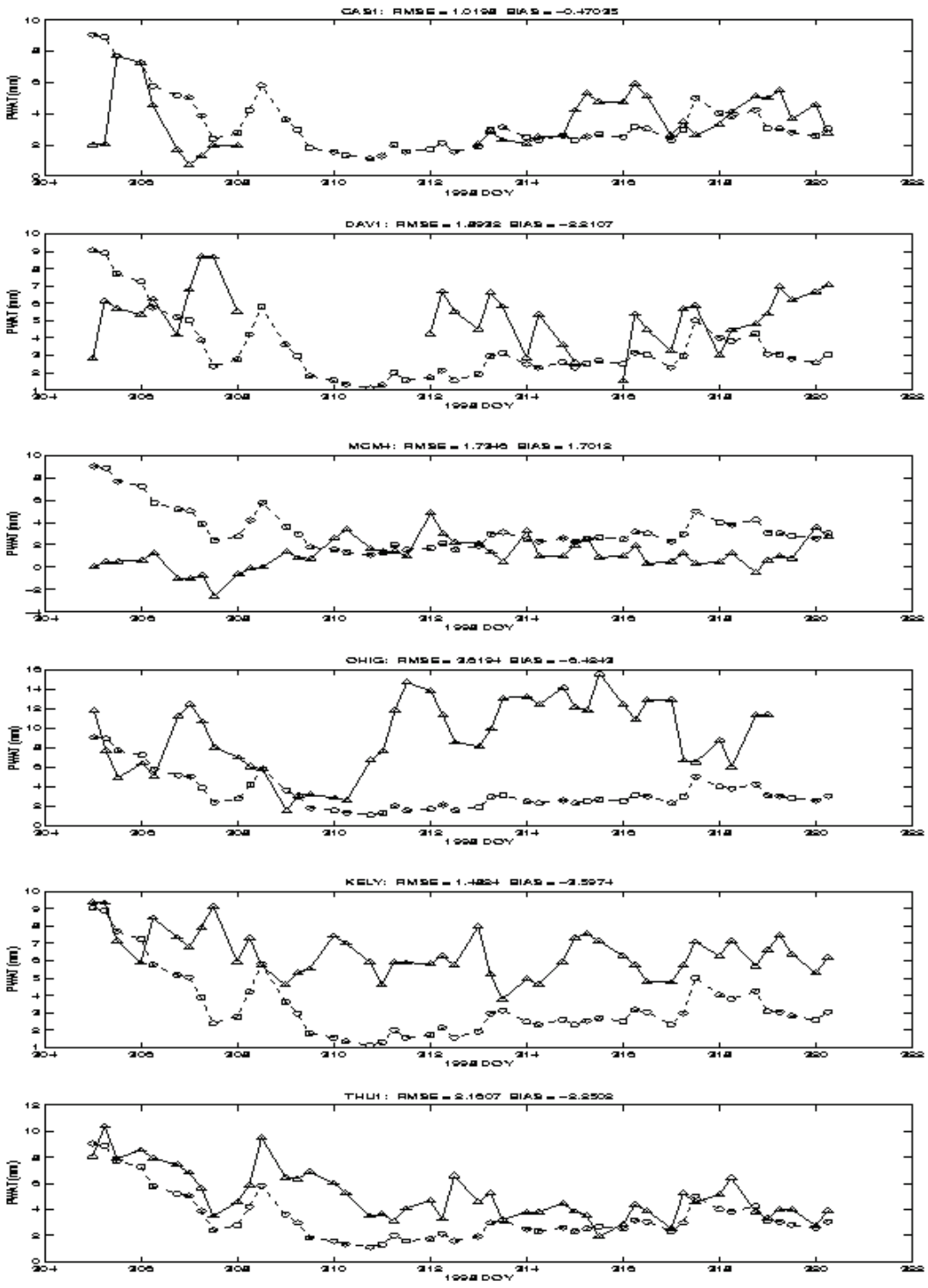

Figure 10. Precipitable water vapor values for various stations. Solid lines with trianges are GPS derived values, dashed lines with circles are NCEP values.

4.0 References

Ambrose, D., Pressure-volume-temperature, in *Recommended Reference Materials for the Realization of Physiochemical Properties*, K. N. Marsh ed., Blackwell Sci. Pub., 73-114, 1987.

Astronomical Almanac, U. S. Government Printing Office, 1999.

Birch, K. P. and M. J. Downs, Corrections to the updated Eldén equation for the refractive index of air, *Metrologia, 31,* 315-316, 1994.

Boer, G. J., K. Arpe, M. Blackburn, M. Deque, W. L. Gates, T. L. Hart, H. le Treut, E. Roeckner, D. A. Sheinin, I. Simmonds, R. N. B. Smith, T. Tokioka, R. T. Wetherald and D. Williamson, Some results from an intercomparison of climates simulated by 14 atmospheric general circulation models, *J. Geophys. Res., 97*, 12771-12786, 1992.

Ciddor, P. E., Refractive index of air: new equations for the visible and infrared, *Appl. Opt., 35,* 1566-1573, 1996.

Ciddor, P. E. and R. J. Hill, Refractive index of air. 2. Group index, *Appl. Opt., 38,* 1663-1667, 1999.

Davis, J. L., T. A. Herring, I. I. Shapiro, A. E. E. Rogers and G. Elgered, Geodesy by radio interferometry: Effects of atmospheric modeling errors on estimates of baseline length, *Radio Sci., 20,* 1593-1607, 1985.

Dongarra, J. J., *LINPACK User's Guide,* SIAM, Philadelphia, 1979.

Eldén, B., The dispersion of standard air, *J. Opt. Soc. Am., 43,* 339-344, 1953.

Eldén, B., The refractive index of air, *Metrologia, 2,* 12-80, 1966.

Fleagle, R. G. and J. A. Businger, *An Introduction to Atmospheric Physics,* Academic, Orlando, FL, 1980.

Harrison, L. P., Fundamental concepts and definitions relating to humidity, in *Humidity and Moisture*, A. Wexler ed, Reinhold Pub. Co., New York, vol. 3, 3-70, 1965.

Harrison, L. P., Imperfect gas relationships, in *Humidity and Moisture*, A. Wexler ed, Reinhold Pub. Co., New York, vol. 3, 3-70, 1965.

Heiskanen, W.A. and H. Moritz, *Physical Geodesy,* W.H. Freeman, San Francisco, 1967.

IUGG (International Union of Geodesy and Geophysics), Resolutions, 13th General Assembly, *Bull. Geodesique, 70,* 390, 1963.

IUGG (International Union of Geodesy and Geophysics), Refractive indices of light, infrared and radio waves in the atmosphere, *IAG Special Commission Report, presented at 22nd General Assembly of IUGG,* 1999.

Kanamitsu, M., Description of the NMC Global Data Assimilation and Forecast System, *Wea. and Forecasting, 4(3)*, 335-342, 1989.

Kanamitsu, M., Alpert, J. C., Campana, K. A., Caplan, P. M., Deaven, D. G., Iredell, M., Katz, B., Pan, H. L., Sela, J., and White, G. H., Recent Changes Implemented into the Global Forecast System at NMC, *Wea. and Forecasting, 6,* 425-435, 1991.

Marini, J. W., Correction of satellite tracking data for an arbitrary tropospheric profile, *Radio Sci., 7*, 223-231, 1972.

Marini, J. W. and C. W. Murray, Correction of laser range tracking data for atmospheric refraction at elevation angles above 10 degrees, *NASA Tech. Rep. X-591-73-351*, 1973.

McGarry, J., Correlation and Prediction of the Vapor Pressures of Pure Liquids over Large Pressure Ranges, *Ind. Eng. Chem. Process Des. Dev., 22*, 313-322, 1983.

Moritz, H., Geodetic Reference System 1980, *Bulliten Geodesique, 54(3),* 395-405, 1980.

National Imagery and Mapping Agency, Department of Defense World Geodetic System 1984: Its Definition and Relationships with Local Geodetic Systems, *NIMA Tech. Rpt 8350.2,* Bethesda, MD, Third Edition 4 July, 1997.

National Oceanic and Atmospheric Administration, U.S. Standard Atmosphere, 1976.

Niell, A. E., Global mapping functions for the atmospheric delay at radio wavelengths, *J. Geophys. Res., 101(B2),* 3227-3246, 1996.

Owens, J. C., Optical refractive index of air: Dependence on pressure, temperature, and composition, *Appl. Opt., 6,* 51-59, 1967.

Parrish, D. F., and Derber, J. C., The National Meteorological Center's Spectral Statistical-Interpolation Analysis System, *Mon. Wea. Rev.*, vol. 120, 1747-1763, 1992.

Peck, E. R. and K. Reeder, Dispersion of Air, *J. Opt. Soc. Am., 62,* 958-962, 1972.

Press, W. H., B. P. Flannery, S. A. Teukolsky, W. T. Vetterling, Numerical Recipes, Cambridge Uni. Press, 1989.

Quinn, K. J., Annual report of the GLAS tropospheric delay science team, 1996.

Rüeger, J. M., *Electronic Distance Measurement - An Introduction*, Springer-Verlag, NY, 1996.

Saastamoinen, J., Atmospheric correction for the troposphere and stratosphere in radio ranging of satellites, in *The Use of Artificial Satellites for Geodesy, Geophys. Monogr. Ser., vol. 15,* edited by S. W. Henriksen, A. Mancini, and B. H. Chovitz, 247-251, AGU, Washington D. C., 1972.

Schutz, B., GLAS Geolocation, *GLAS Algorithm Theoretical Basis Document,* Uni. Texas, 1999.

Stackpole, John D., The WMO Format for the Storage of Weather Product Information and the Exchange of Weather Product Messages in Gridded Binary Form, *NOAA Office Note 388,* 1994.

Steffen, K., J. E. Box, and W. Abdalati, Greenland Climate Network: GC-Net, *in Colbeck, S. C. Ed. CRREL 96-27 Special Report on Glaciers, Ice Sheets and Volcanoes, trib. to M. Meier*, 98-103, 1996.

Stearns, C. R., and G. Wendler, Research results from Antarctic automatic weather stations, *Rev. Geophys., 26 (1)*, 45-61, 1988.

Trenbreth, K. E. and J. G. Olsen, An evaluation and intercomparison of global analyses from the National Meteorological Center and the European Centre for Medium Range Weather Fore-

casts, *Bull. Am. Met. Soc, 69,* 1047-1057, 1988.

Appendix A – ICESat Mission Outline

The Ice, Cloud and land Elevation Satellite (ICESat) was launched on 13 January 2003. The Geoscience Laser Altimeter System (GLAS) instrument onboard ICESat made its first laser elevation measurement of the Earth on 21 February 2003 and its last on 11 October 2009. The three lasers employed by GLAS did not perform as long as expected, and following the failure of Laser 1 on 5 March 2003 the ICESat mission was modified to meet the requirement for capturing a multi-year time series of ice sheet elevations (Schutz et al., 2005). For the modified mission scenario, the spacecraft entered a 91-day repeat science orbit (compared to a planned 183-day repeat) and the lasers were activated for about 33 days of this 91-day repeat, two or three times per year. This campaign mode operation is summarized in Table A.1, and other significant parameters and events are listed in Table A.2. ICESat laser campaigns are designated by a laser number (L1, L2 or L3), followed by a letter in the sequence of operation. Following campaign L2f, attempts to restart any of the lasers were not successful. The spacecraft was put through a series of engineering tests in early 2010. De-orbit maneuvers were carried out in June and July 2010. The spacecraft was "passivated" on 14 August and reentered the Earth's atmosphere on 30 August 2010 over the Barents Sea northeast of Norway.

Table A.1: ICESat Laser Operation Campaigns

Campaign	Year	Day of year	Calendar Dates	Number of days (d)	Repeat orbit (d)	Repeat tracks[1]
L1a	2003	051-088	20 Feb-21 Mar	37	8	001-072 to 006-023
L2a	2003	268-277/ 277-322	25 Sep-4 Oct/ 4 Oct-21 Nov	54	8/ 91	028-088 to 029-100/ 1098 to 0421
L2b	2004	048-081	17 Feb-21 Mar	33	91	1284 to 0421
L2c	2004	139-173	18 May-21 Jun	34	91	1283 to 0434
L3a	2004	277-313	3 Oct-8 Nov	37	91	1273 to 0452
L3b	2005	048-083	17 Feb-24 Mar	35	91	1258 to 0426
L3c	2005	140-174	20 May-23 Jun	34	91	1275 to 0421
L3d	2005	294-328	21 Oct-24 Nov	34	91	1282 to 0421
L3e	2006	053-087	22 Feb-28 Mar	34	91	1283 to 0424
L3f	2006	144-177	24 May-26 Jun	33	91	1283 to 0421
L3g	2006	298-331	25 Oct-27 Nov	33	91	1283 to 0423
L3h	2007	071-104	12 Mar-14 Apr	33	91	1279 to 0426
L3i	2007	275-309	2 Oct-5 Nov	34	91	1280 to 0421
L3j	2008	048-081	17 Feb-21 Mar	33	91	1282 to 0422
L3k	2008	278-293	4 Oct-19 Oct	15	91	1283 to 0145
L2d	2008	330-352	25 Nov-17 Dec	22	91	0096 to 0423
L2e	2009	068-101	9 Mar-11 Apr	33	91	1286 to 0424
L2f	2009	273-284	30 Sep-11 Oct	11	91	1280 to 0084

[1] There are 119 tracks in the 8-day orbit and 1354 tracks in the 91-day orbit. Cycle numbers are included for the 8-day repeat periods.

Table A.2: Significant ICESat Parameters and Events by Campaign

Cam-paign	Year	Day of year	S/C orient-ation[1]	Start Beta' Angle (º)	End Beta' Angle (º)	Start Laser Infrared Energy (mJ)	End Laser Infrared Energy (mJ)	Mean footprint major axis (m)	Day of year – comments
-	2003	013	-	-	-	-	-	-	013 – launch
L1a	2003	051-088	-Y/+X	-45	-32	72	51	149	080 – yaw flip 085 – safe hold, adjust temperature
L2a	2003	268-277/ 277-322	+Y	51	69	80	55	100	277 – orbit change 286 – laser temperature anomaly 287, 302 – adjust temperature 311 – GPS solar flare anomaly
L2b	2004	048-081	+Y	54	40	57	33	90	
L2c	2004	139-173	-X	13	-4	33	5	88	142-147 – adjust temperature
L3a	2004	277-313	-Y	-48	-58	67	62	56	293 – adjust temperature
L3b	2005	048-083	-Y	-56	-45	68	54	80	054 – suspected amplifier bar drop, begin footprint anomaly[2] 068 – suspected amplifier bar drop
L3c	2005	140-174	+X	-20	-4	49	44	55	
L3d	2005	294-328	+Y	51	63	43	39	52	
L3e	2006	053-087	+Y	62	48	38	30	52	
L3f	2006	144-177	-X	20	4	30	30	51	149 - Energy jump up 2mJ
L3g	2006	298-331	-Y	-44	-54	30	24	53	310 – begin ITRF 2005
L3h	2007	071-104	-Y	-60	-47	24	21	56	
L3i	2007	275-309	+Y	32	46	22	20	57	
L3j	2008	048-081	+Y	74	62	20	16	59	
L3k	2008	278-293	+X	-28	-32	18	12	52	289 – Energy drop 4 mJ
L2d	2008	330-352	-Y	-45	-53	8	4	-	343-344 – adjust temperature, energy up 5 mJ
L2e	2009	068-101	-Y	-71	-59	6	2	-	094-095 – adjust temperature
L2f	2009	273-284	-X	20	25	4	2	-	
-	2010	242	-	-	-	-	-	-	242 – reentry

[1] The spacecraft is said to be in "Sailboat" mode for ±Y orientations and in "Airplane" mode for ±X orientations, where the direction indicates the solar panel orientation with respect to the spacecraft velocity using the GLAS coordinate frame.

[2] The footprint diameter during L3b changed from a mean of 54 m (day of year 048-053) to 84 m (055-068). The reason for the larger footprint size during the latter part of the campaign is unknown, although a suspected amplifier bar dropout occurs near the event.

References

Schutz, B.E.; Zwally, H.J.; Shuman, C.A.; Hancock, D.; DiMarzio, J.P. Overview of the ICESat Mission. *Geophysical Research Letters* **2005**, 32, L21S01 (DOI:10.1029/2005GL024009).

Appendix B Off-Nadir Atmospheric Delay Corrections Addendum

The atmospheric delay calibration ATBD discussed the effects of off-nadir pointing on the atmospheric delay correction and concluded that for pointing within 15° of nadir, a simple 1/sin(elevation angle) formulation would be provide a sub-millimeter accuracy corrections. Since it now seems likely that ICESat might point as far as 35o off-nadir, we have revaluated this approximation for large off nadir angles (up to 35°). The geometry for relating off-nadir angle, θ, to zenith angle, z=90-elevation angle (ε), is shown in Figure 1.

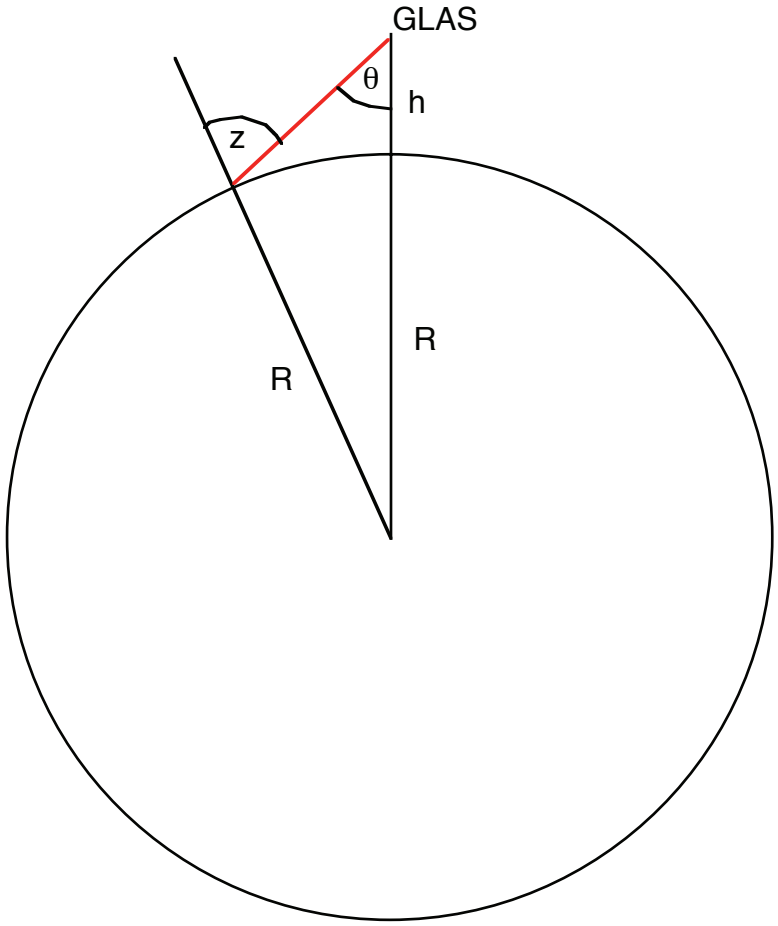

Figure 1: Geometry relating nadir angle to elevation angle. R is the radius of the Earth (~6378 km); h is the altitude of the satellite (~600km); θ is the nadir angle; and z is the zenith angle, which equals 90-ε, where e is the elevation angle. For q=35°, z=38.868° and e=51.132°.

The comparison here we used the Niell [1996] hydrostatic mapping function that relates the atmospheric delay in the zenith direction to the delay at a specified (in-vacuum) elevation angle. The form of the mapping function is a continued fraction in sin(e). With the coefficients appropriate for polar regions the Niell mapping function takes the form:

$$\Delta L = m(\varepsilon)\Delta L_Z$$

$$m(e) = \frac{1/(1 + a/(1 + b/1 + c)))}{\sin(\varepsilon) + a/(\sin(\varepsilon) + b/(\sin(\varepsilon) + c)))} \quad (1)$$

where ΔL is the atmospheric delay at elevation angle, ε; ΔL_z is the delay in the zenith direction. For Polar Regions, under average conditions, a=1.2046x10^{-3}, b=2.90249x10^{-3}, and c=64.258x10^{-3}.

Figure 2, shows the values of ΔL, for ΔL_z=2.3m as a function of off-nadir angle for m(ε) given in equation (1) and m(ε) given simply by 1/sin(ε). At this scale, the differences are difficult to see. In Figure 3, we show the difference in units of mm. At the largest off-nadir angle, the difference is <2.5 mm and well within the atmospheric delay model error budget,

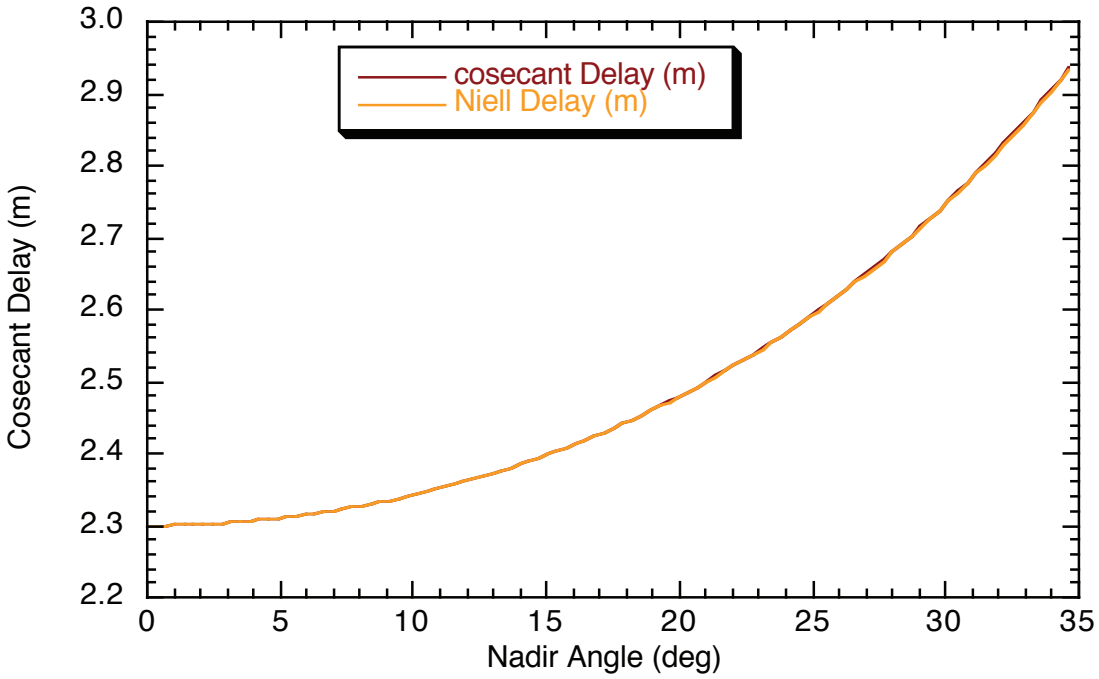

Figure 2: Atmospheric delay as function of off-nadir angle under nominal conditions given in the text. Units are meters.

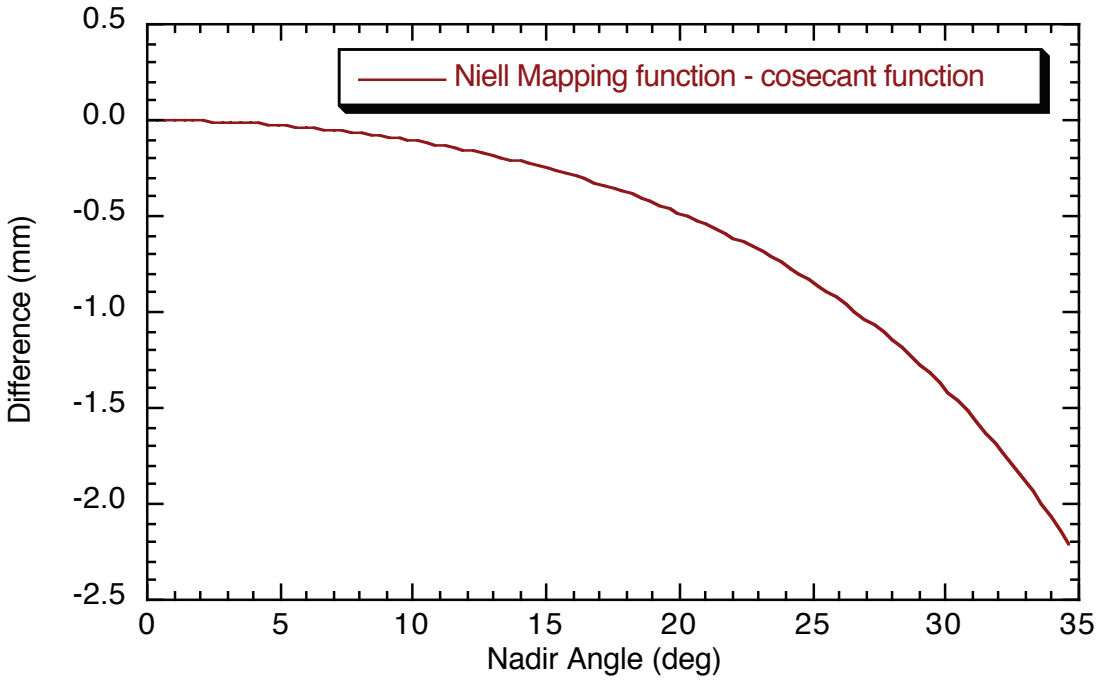

Figure 3: Difference between the Niell mapping function and the cosecant mapping function under nominal conditions. Difference units are millimeters.

Bending effects

The effects of bending were approximately evaluated in the ATBD for off-nadir angles up to 15o. We have more carefully considered these effects here because the off-nadir angles could be as large as 35º. To evaluate the effect we ray-traced through a standard, spherically symmetric, atmospheric model keeping careful track of the bending angles and the deviation between the vacuum and refracted paths. The ray tracing was performed from the ground to the satellite (at 600 km altitude) since this approach tends to more numerically stable than ray tracing from vacuum into the Earth's atmosphere. The ray tracing started at a series of elevations ranging between 90 and 50 degrees. From the ray-trace, the nadir angle at the satellite and the angle subtended by the arc between initial starting point and the position of ray when it reached 600 km were computed. In addition, we also integrated the atmospheric delay and the bending angle as checks on the ray-trace. The differences between the atmospheric delays computed from the ray-trace and those given by the simply cosecant law were indistinguishable from those shown in Figure 3 above. The bending angle matched the values given be the Astronomical Almanac [1999] formula in the ATBD to within one milli-degree.

Figure 4 show the arc distance to the footprint from the sub-satellite point computed from the ray tracing and from simple in vacuum geometry. Figure 5 shows the difference. In the worst case, the difference in foot print location is less than 5 meters and we conclude that atmospheric bending effects on foot print location can be ignored even for the largest

off nadir pointing angles. Intuitively these results make sense when it is realized that most of the bending occurs in the lowest 10km of the atmosphere, and for a bending angle of 0.014 degrees from 10 km altitude, the foot print displacement would be 3.2 m for a ray at 50° deg elevation angle.

Figure 4 also shows that for a 94° inclination orbit (sub satellite point ~440 km from the pole, that a nadir angle of ~35° will be needed to range to the pole.

Conclusions

Based on these calculations, we recommend that a simple $1/\sin(\varepsilon)$ where ε is given by $\cos^{-1}(\sin(\theta)R_g/R_s)$ and R_g is the radius at the footprint and R_s is the radius to ICESat. To <5 meters, the bending of the ray by the atmosphere can be neglected in geo-locating the footprint.

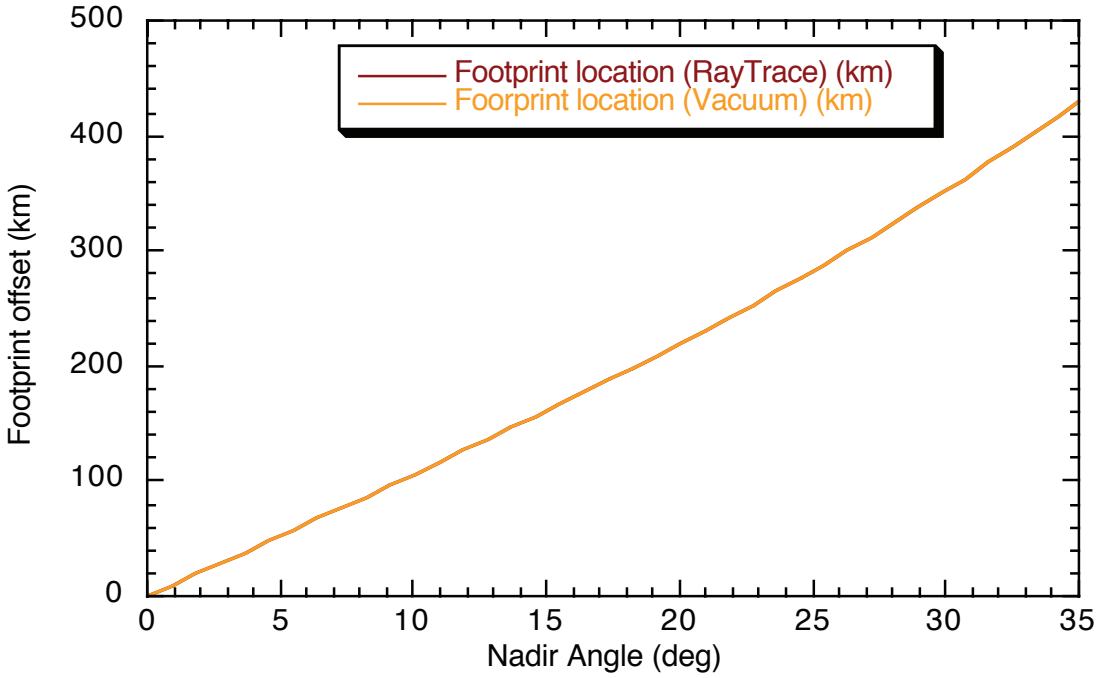

Figure 4: Distance between the foot print location and the sub-satellite point as a function of nadir angle computed in vacuum and by ray tracing through a standard atmospheric delay model.

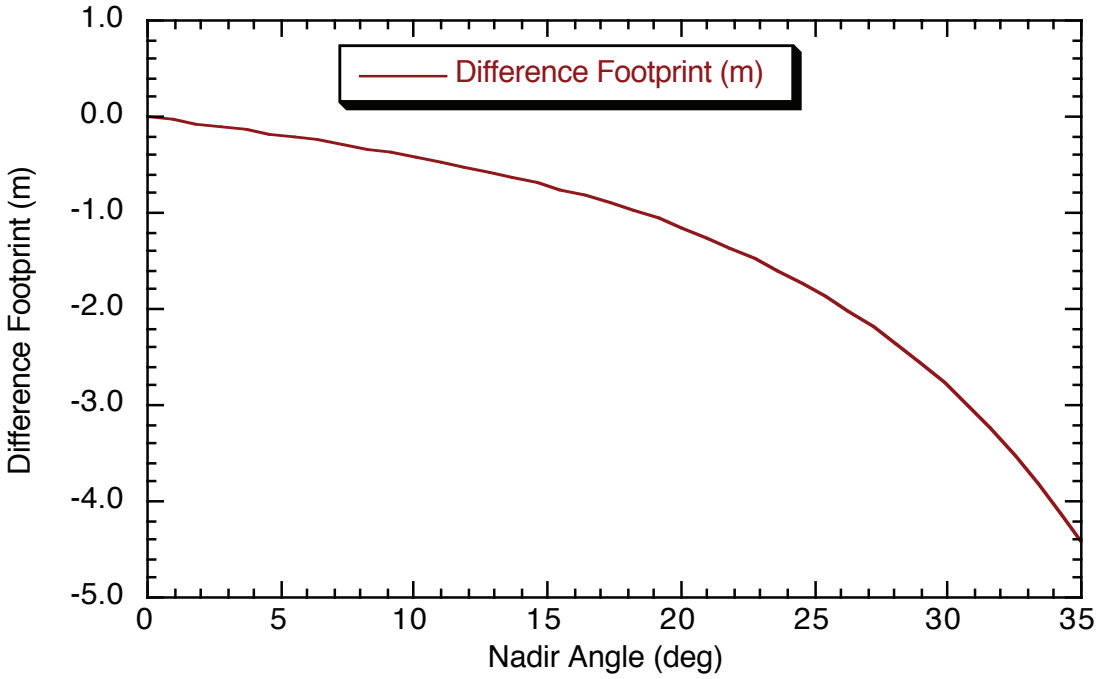

Figure 5: Difference between the two curves in Figure 4 shown in meters.

References

Astronomical Almanac, U. S. Government Printing Office, 1999.

Niell, A. E., Global mapping functions for the atmospheric delay at radio wavelengths, *J. Geophys. Res., 101*(B2), 3227-3246, 1996.

REPORT DOCUMENTATION PAGE

Form Approved
OMB No. 0704-0188

1. REPORT DATE *(DD-MM-YYYY)*	2. REPORT TYPE	3. DATES COVERED *(From - To)*
30-10-2012	Technical Memorandum	

4. TITLE AND SUBTITLE

The Algorithm Theoretical Basis Document for the Atmospheric Delay Correction to GLAS Laser Altimeter Ranges

5a. CONTRACT NUMBER

5b. GRANT NUMBER

5c. PROGRAM ELEMENT NUMBER

6. AUTHOR(S)

Thomas A. Herring, Katherine J. Quinn

5d. PROJECT NUMBER

5e. TASK NUMBER

5f. WORK UNIT NUMBER

7. PERFORMING ORGANIZATION NAME(S) AND ADDRESS(ES)

The Massachusetts Institute of Technology, Cambridge, MA

Goddard Space Flight Center
Greenbelt, MD 20771

8. PERFORMING ORGANIZATION REPORT NUMBER

9. SPONSORING/MONITORING AGENCY NAME(S) AND ADDRESS(ES)

National Aeronautics and Space Administration
Washington, DC 20546-0001

10. SPONSORING/MONITOR'S ACRONYM(S)

NASA GSFC

11. SPONSORING/MONITORING REPORT NUMBER

NASA/TM-2012-208641/Vol. 8

12. DISTRIBUTION/AVAILABILITY STATEMENT

Unclassified-Unlimited, Subject Category: 2, 43, 47
Report available from the NASA Center for Aerospace Information, 7115 Standard Drive, Hanover, MD 21076. (443)757-5802

13. SUPPLEMENTARY NOTES

14. ABSTRACT

NASA's Ice, Cloud, and Land Elevation Satellite (ICESat) mission will be launched late 2001. It's primary instrument is the Geoscience Laser Altimeter System (GLAS) instrument. The main purpose of this instrument is to measure elevation changes of the Greenland and Antarctic icesheets. To accurately measure the ranges it is necessary to correct for the atmospheric delay of the laser pulses. The atmospheric delay depends on the integral of the refractive index along the path that the laser pulse travels through the atmosphere. The refractive index of air at optical wavelengths is a function of density and molecular composition. For ray paths near zenith and closed form equations for the refractivity, the atmospheric delay can be shown to be directly related to surface pressure and total column precipitable water vapor. For ray paths off zenith a mapping function relates the delay to the zenith delay. The closed form equations for refractivity recommended by the International Union of Geodesy and Geophysics (IUGG) are optimized for ground based geodesy techniques and in the next section we will consider whether these equations are suitable for satellite laser altimetry.

15. SUBJECT TERMS

Cryospheres, remote sensing, geodesy, satellite instruments, lasers, altimetry, refraction, elevation, algorithms, ice sheet elevation, ice environments, ice

16. SECURITY CLASSIFICATION OF:			17. LIMITATION OF ABSTRACT	18. NUMBER OF PAGES	19b. NAME OF RESPONSIBLE PERSON
a. REPORT	b. ABSTRACT	c. THIS PAGE			Dr. H. Jay Zwally
Unclassified	Unclassified	Unclassified	Unclassified	47	19b. TELEPHONE NUMBER *(Include area code)* (301) 614-5643